Deliverable Report for Grant Agreement Number 760813

Deliverable 1.2

ENM dispersibility and physicochemical exposure relevant properties

Due date of deliverable: 30/04/2020

Actual submission date: 28/04/2020

Lead beneficiary for this deliverable: *ISTEC-CNR*

Dissemination Level:		
PU	Public	X
PP	Restricted to other programme participants (including the Commission Services)	
RE	Restricted to a group specified by the consortium (including the Commission Services)	
CO	Confidential, only for members of the consortium (including the Commission Services)	

Table of Contents

1. Description of task

Task 1.2 Measured and modelled ENM dispersion, transport and realistic dose exposure characteristics; (**ISTEC**, UNamur, NRCWE, KRISS, BASF); **M2-28**

This task will assess properties that affect dispersion, particle exposure and transport related processes, monitoring phenomena occurring at nano-liquid and nano-air interphases. Fundamental transformation and behaviour occurring in (eco)toxicologically relevant media will be evaluated by focusing on several end-points

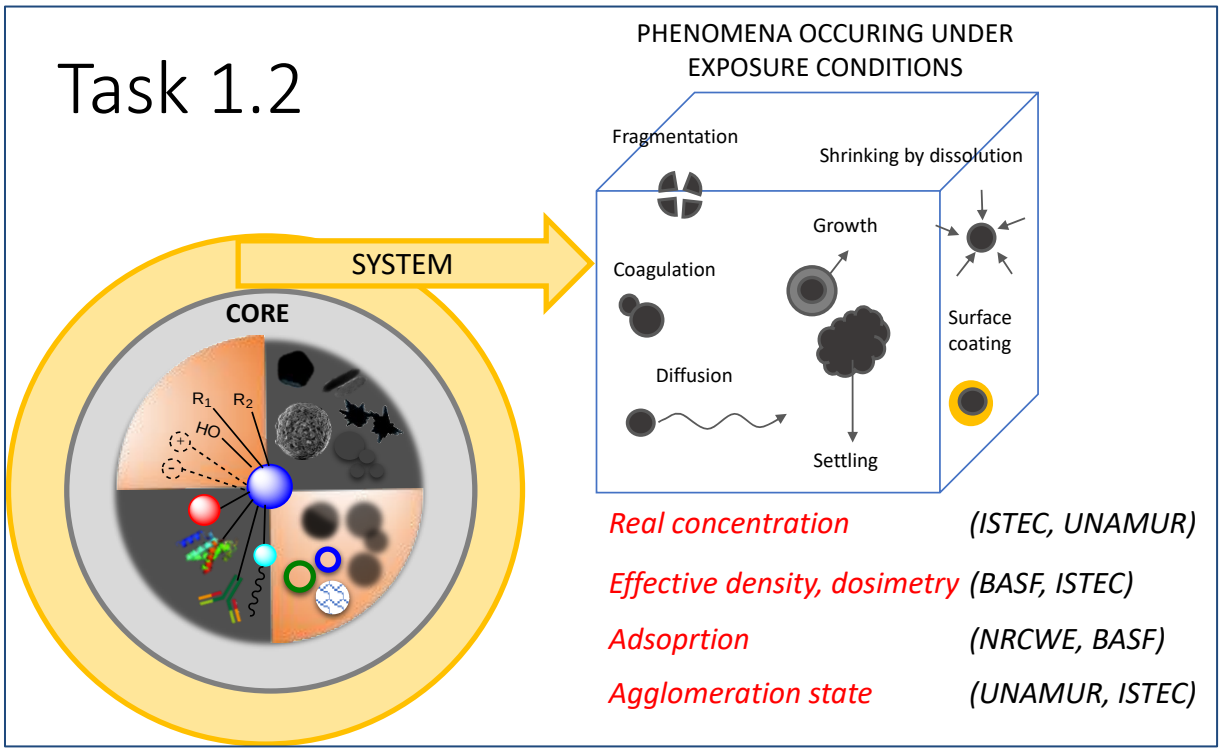

as reported in Fig 1.

Figure 1- System dependent properties characterised in PATROLS Task 1.2

The factors controlling the dispersibility and settling of ENM will be studied in relevant liquid media after dispersion using the harmonized probe-dispersion protocol developed in NANoREG (D2.08 and D2.0973), while determination of aggregate/agglomerate size-distribution and density will be established using e.g., Dynamic Light Scattering (DLS) and Centrifugal Liquid Sedimentation (CLS) methods

or other suitable techniques dependent upon ENM type (BASF, NRCWE, KRISS, UNamur). Evolution of the surface and bulk composition in (eco) tox relevant media will be determined with the XPS and PIXE techniques (UNamur). Settling rate at gravity will be assessed for relevant exposure media using a Centrifugal Separation Analysis (CSA) and for sub-10-nm ENM also Analytical Ultracentrifugation (AUC) techniques, applying Relative Centrifugal Force adjustable. between 1g and 250,000g (BASF, KRISS). Zeta potential and isoelectric points will be assessed by ISTEC using ELS, with increasing complexity of co-exposures from salts to protein components. An electrokinetic technique, more suitable for working with opaque or concentrated suspensions (stock suspensions) will be used for comparison. The role of hydrophobicity - hydrophilicity will be evaluated based on data provided by ISTEC using sessile water drop contact angle for a rapid screening of hydrophobicity and measuring enthalpy of interaction with water molecules if more sophisticated investigation on mechanism related to surface affinity occurs. The amount of adsorbed biomolecules and ions will be assessed by depletion analysis of specific substances in test mediums using pure media as a reference (NRCWE). All relevant data will be compiled and analysed to identify the relative roles of the different modifiers in dispersion-settling models and to understand the effects of such interactions on the availability (dosimetry) of ENM, as they can potentially compete with diffusion, aggregation, sedimentation, (partial) dissolution and surface transformation (ISTEC and NRCWE). Dustiness data are now identified by ECHA as a critical grouping criterion and for predictive assessment of particle exposure by modelling. Tests will be conducted on powders using the Small Rotating Drum (SRD) dustiness method (pre-EN standard) to assess the respirable mass-based dustiness (cyclone) and number dustiness indexes (CPC), as well as the dustiness kinetics (CPC) and aerodynamic dust size-distribution by ELPI (NRCWE, BASF). Offline morphological analyses will be

made by TEM. The data will be used to assess the potential alveolar inhalation exposure and exposure dose through modelling (NRCWE). Data collected and generated will be communicated to WP6, Task 6.1 for curation in the PATROLS database.

2. Description of work & main achievements

Abstract

In response to WP1 specific objective: “Fit for purpose characterisation of physicochemical properties to support test specific exposure, fate and dosimetry assessment”, the WP1 focused the characterisation on two main issues that govern the dose, once NPs come in contact with the biological environment. The first issue is addressed in Section 2.2. Here we report the results of the characterisation, mimicking the NPs (NPs) exposure in in-vitro testing conditions and in in-vivo simulant fluids. Whilst Section 2.3 investigates “how much” of the dose is actually delivered in in-vitro experimental models, collecting data to be used as input and for the experimental validation of the well-known 2D dosimetry model (DG model), such as particle size distribution and sedimentation rate. Here we also reported the results of single particle inductively coupled plasma mass spectrometry (SP-ICP-MS) analysis applied to AgNPs dispersion in in-vitro relevant media, with an estimation in situ of the amount of AgNPs and ionic Ag^+ fraction, avoiding destructive ultrafiltration pre-treatments. Finally, in Section 2.4 we reported materials and methods, standard operating procedures (SOP) used or proposed for completion of the described case studies.

2.1 Introduction

Physico-chemical properties are key starting points for risk assessment of chemicals. They provide a description of the chemical, and prove useful in assessment of environmental behaviour, uptake routes into organisms, toxicokinetics and ultimate effects in organisms. Any attempt to compare the utility, or efficacy, of an ENM for a specific application, or to assess its potential harmful effects requires that the material be adequately characterized for all properties that are relevant to the specific purpose/end use, in the relevant environment (Gubala et al., 2018). Two main issues

have been investigated over the past few years in order to understand and quantify ENM biological effects (Krug, 2014). The first deal with ENM biological identity; how ENM transform when introduced in biologically relevant media and face the biological targets. The second concerns how many nanoparticles (NPs) interact with biological targets and are taken up by cells (*in vitro*) or organisms (*in vivo*) in order to derive benchmark doses. Fundamental consideration has to be made about the unique kinetics of these materials when dispersed in their use or testing matrices. Particles in general and NPs specifically are dynamic systems, they diffuse, settle, and agglomerate in their dispersing medium as a function of systemic and particle properties: media density and viscosity, particle size, shape, density, surface charge and hydrophobicity (Teeguarden et al., 2007). Cellular dose is then a function of these factors as they determine the amount and rate of transport of NPs to cells in culture media.

2.2 "What" is dosed: sample dispersion governs the exposure identity

a. Fresh / Freeze-thawed / Aged suspensions and stability tests

Full physicochemical characterisation is mandatory to establish the hazard potential and guide the decision as to whether ENM need additional tests *in vivo*. A NANoREG Protocol was developed as a standard operating procedure to produce consistent and repeatable nanoparticle dispersions of ENMs for nanotoxicological studies, based on previous work in e.g., the EU FP7 ENPRA and EAHC NANOGENOTOX projects.

To reach the highest possible level of comparability in the studies in the different laboratories, it was found that the users would benefit greatly from benchmark values. Therefore, a set of such benchmark values were generated and summarized in Table 1.

Table 1. Benchmark hydrodynamic average Zeta-size (Z_{ave}) and PDI values for batch dispersions prepared following the NANOGENOTOX and ENPRA dispersion protocols.

Test material	NANOGENOTOX SOP	ENPRA SOP
	Z_{ave} [nm] / PDI (n analysis)	**Z_{pot} [mV]**
TiO_2 NM-105 / JRCBN01005a	155±1 / 0,1 (n=3x10) *	-34±0,4 §
TiO_2 E171	348±21 / 0,2 (n=3x10) §	-0,3±0,3 §
ZnO NM-110 / JRCNM01100a	233,1±2,6 / 0,1 (n=3x10) *	-31±0,2 §
ZnO NM-111 / JRCNM01101a	244,8±4,2 / 0,1 (n=3x10) *	-22±0,4 §
SiO_2 NM-200 / JRCNM02000a	250,6±19,7 / 0,4 (n=11x10) *	-40±2 §
SiO_2 IUF (Sigma Aldrich)	225±4 / 0,3 (n=3x10) §	-41±0,6 §
CeO_2 NM-212 / JRCNM02102a	240,7±12,2 / 0,2 (n=3x10) *	-37±2 §
Ag NM-300K	79,9±0,7 / 0,3 (n=3x10) *	-10±0,5 §
Ag-Sigma	235±8 / 0,4 (n=3x10) §	-38±1 §
MWCNTs NRCWE-006 /	967±41 / 0,3 (n=3x10) *	-35±0,5 §

*NRCWE data; §ISTEC data

While the NANOGENOTOX probe-dispersion protocol is straightforward and the required equipment is standard across most nanotoxicology labs, it can be a wasteful procedure if only small volumes are needed as a fresh dispersion is needed for each experiment. The NANOGENOTOX protocol produces 6 mL of particle dispersion at a

concentration of 2.56 mg/mL sufficient for approximately 30 x 96-well microwell plates with sufficient *in vitro* exposure concentrations for each dispersion. Moreover, high-throughput testing usually requires testing of several materials at the same time, and in this case a “one-after-the-other” preparation of each dispersion will be time-consuming (typically 10 – 20 minutes per sonication depending on equipment and 5 minutes between samples). For this type of high-through-put testing, the “one-after-the-other” approach is not recommended, because it would result in dispersion-to-rest for an extended duration of time risking extensive dissolution and loss of reactivity. Consequently, a previously used laboratory method of quench-freezing sub-sampled aliquots of batch dispersions for later testing (Danielsen et al., 2011; Jacobsen et al., 2009) was officially tested by comparative physicochemical analysis and in vitro studies in NANoREG by testing on NM-102; NM-11NM-300K, NM-401; Sigma nano-ZnO, and Sigma nano-CeO_2 (Vila et al., 2017).

In this work, the application and potential consequence of quench-freezing batch dispersions for re-use upon thawing was further investigated and documented on the broader suite of materials tested in PATROLS.

The colloidal characterization (DLS mean diameter and ELS Zeta potential) of fresh (FR), freeze-thawed (FT) and aged (A) suspensions was performed and their colloidal stability tested in order to assess the suitability of different preparation and storing conditions. In Section 2.3, the suitability of freeze-thawing treatment was also tested, measuring size distribution and deriving further input parameters to be used in the Distorted Grid (DG) dosimetry model developed by DeLoid (DeLoid et al., 2017, 2015). In this way it was possible to assess more directly the effect that the freeze-thawing strategy had on the calculated deposited dose. The hydrodynamic mean diameter of fresh stock suspensions where compared with those of freeze-thawed and aged suspensions, as reported in Figure 2.

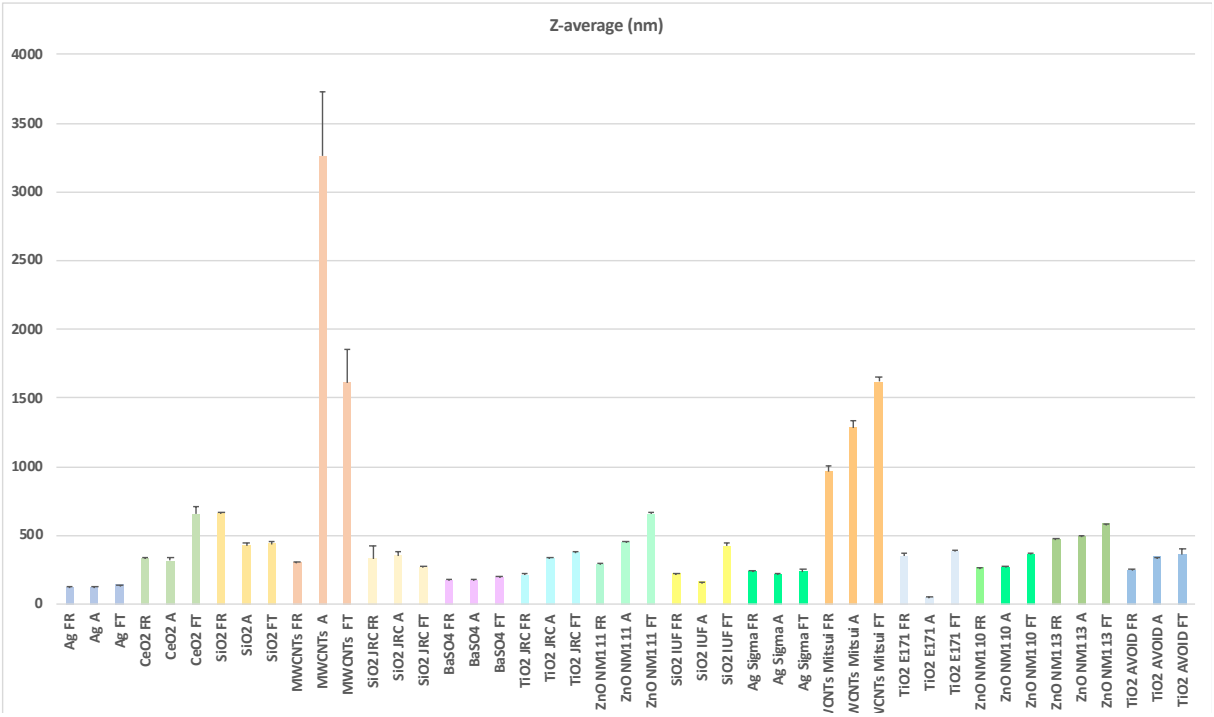

Figure 2. DLS mean diameter of fresh (FR), freeze-thawed (FT) and aged (A) stocks suspensions

Some samples like Ag NM300K, Ag Sigma, $BaSO_4$ and SiO_2 NM200 seem to be only slightly affected by freezing (-80°C) or ageing at storing conditions (4°C). In contrast, some samples such as MWCNTs NM402 and Mitsui are dramatically destabilized, while other samples like TiO_2 and ZnO are only partially modified and in general become more aggregated after freeze-thawing treatment. Overall, considering the advantages that freeze-thawing treatment can provide for speeding the characterizations process, we can conclude that this can be considered a good option to save time and allow a better comparison between samples prepared in different times.

Figure 3 reports the comparison of zeta potential of stock suspensions in order to check if aggregation occurring after treatments at 80°C (FT) or 4°C (A), could affect Zeta potential. Overall the Zeta potential appears to not be affected by post-treatments, confirming once again that freeze-thawing could be a good option for storing and

characterizing samples prepared at different times..

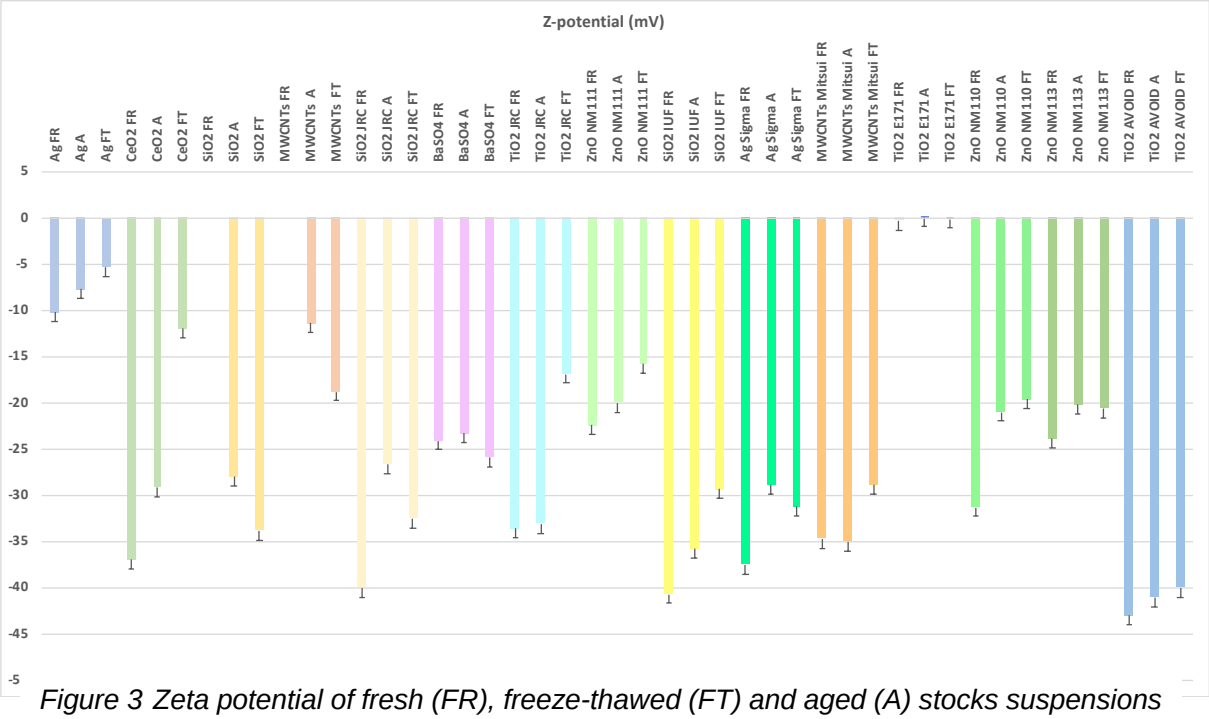

Figure 3 Zeta potential of fresh (FR), freeze-thawed (FT) and aged (A) stocks suspensions

b. Adsorption via depletion analysis

Following the NANOGENOTOX dispersion SOP, test materials are brought into a homogeneous batch dispersion using a medium of highly pure 0.05% sterile-filtered Bovine serum albumin (BSA) water after pre-wetting with a small amount of ethanol. The ethanol is used to pre-separate and lower the surface tension of hydrophobic materials. The BSA-water dispersion medium is constructed to have different functions depending on the type of test material and thereby general applicability. BSA is the main active ingredient and will normally work as a dispersant and/or steric or depletion (polymeric) stabilizer alone or in combination with the overall electrosteric properties of the BSA-water. In many cases stabilization may in fact be achieved by a combination of mechanisms as depicted in Figure 4 and not by single mechanisms.

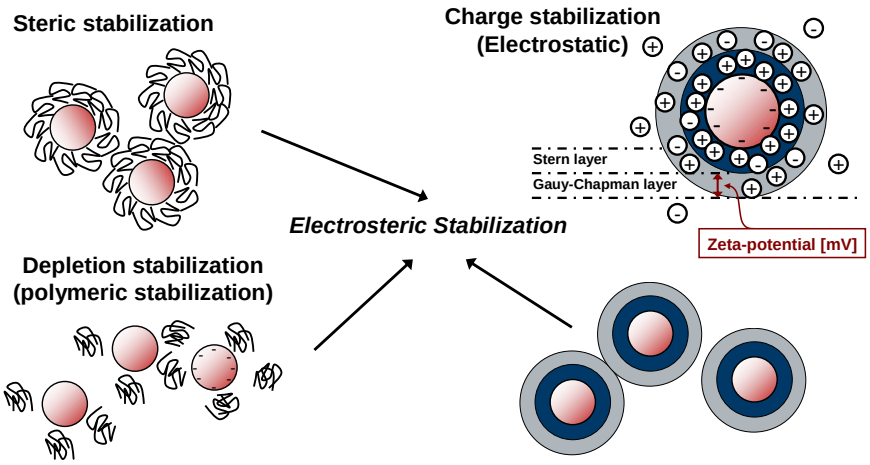

Figure 4. Principle mechanisms for stabilization of suspensions (Monteiro-Riviere and Tran, 2014)

A consequence of using protein-assisted dispersion protocols is that the dose will include a small amount of protein. In toxicological studies this protein is often considered to adhere (coat) entirely the dispersed particles. However, according to the intended function of the protein-assisted dispersion protocol, the protein may be freely accessible or fully adsorbed onto the ENMs' surface. Some studies have shown that protein coatings can affect the uptake and transport properties of nanomaterials. *In vivo*, minor differences are generally observed in pulmonary toxicity after day 1 using different dispersion protocols (Hadrup et al., 2017). *In vitro*, some authors have claimed considerable effects on their toxicological results due to the presence of proteins in the batch dispersion (Marucco et al., 2019; Vranic et al., 2017). While most *in vitro* nanotoxicological researchers have focused on the potential influence of proteins in the dispersion mediums on the toxicological test results, little focus has been set on the potential role of proteins usually present in the cell mediums. Furthermore, even less focus has been given to the potential interaction between test materials and the cytokines and LDH secreted from cells during inflammation and cell membrane leakage, respectively. Recently, it was shown that considerable amounts of LDH, but not IL-6 and IL-8, adsorbs non-specifically onto ZnO in an HAMs F12 with 10% FBS

affecting the ability to determine the in vitro cytotoxicity of ZnO correctly using standard ELISA cytotoxicity assays (Da Silva et al., 2019). In on-going work, we have demonstrated that IL-6 and IL-8 also may adsorb onto some other test materials in HAMs F12 cell nutrient medium (Deliverable 2.08 NANoREG).

The aim of this study is to investigate the full protein-interaction pattern for the PATROLS test materials in all the way, from preparing the batch dispersion with BSA-water, addition into a cell medium with FBS, and finally potential interaction between inflammatory signal proteins (IL-6 and IL-8) and cytoplasmic LDH. The tests were conducted in DMEM plus 10% (w/v) FBS (cDMEM), which is a widely used as complete cell nutrient mixture and the standard experimental test medium in Task 1.2. Only the results of interaction between ENM and LDH are shown in Figure 5, the other results are pending due to Covid-19 emergency and lock-down of experimental activity.

Interaction with IL6, IL-8 and LDH in cDMEM

The results showed a clear loss of LDH in experiments with ZnO (NM-110, NM-111, and NM-113), Ag (Ag-sigma and NM-302 (replacement of expired NM-300K)) and to a minor extent with MWCNT (NM-402) (Figure 5). The LDH adsorption is highly similar between the three ZnO materials ending at around 60% loss of all LDH available in the medium. This pattern reflects the previously identified non-specific adsorption profile for LDH on NM-110 and NM-111 by Da Silva et al. (2019). The silver materials display two different adsorption phenomena. A very high loss is observed at low particle doses of Ag-Sigma while a slower adsorption rate is observed for NM-302. In relation to NM-302, the medium control shows no adsorption of LDH and it can be concluded that the LDH is lost due to interaction with the nanomaterials and not the dispersion medium.

Table 2. Results from analysis of protein and LDH adsorption studies in the NANOGENOTOX batch dispersion medium and cDMEM.

%OD_{LDH} Dose [µg/mL]	E-171	NM-105	Ag-Sigma	NM-302	NM-302DIS	NM-200	IUF-silica	DQ12	NM-110	NM-111	NM-113	NM-212	NM-220	NM-400	NM-402	NRCWE-006
0	0,0	0,0	0,0	0,0	0,0	0,0	0,0	0,0	0,0	0,0	0,0	0,0	0,0	0,0	0,0	0,0
10	0,5	-0,8	37,2	-1,0	-1,3	0,7	0,5	-0,3	50,8	48,1	47,5	-1,3	1,2	-0,6	1,0	-1,4
20	1,5	0,5	53,1	0,1	-3,0	0,3	-1,1	-1,5	56,1	55,3	56,1	0,0	1,2	-0,1	0,8	-1,6
40	-2,2	-0,3	60,4	-0,4	-3,0	-1,5	-1,6	-1,0	56,6	55,7	57,6	-0,6	-0,9	-0,2	0,0	-4,0
80	-1,7	-4,1	69,2	2,4	-3,4	0,5	-4,1	1,5	57,6	56,4	58,2	-2,0	-0,9	-2,3	-1,3	-3,1
160	-0,1	-0,3	79,1	12,0	-2,3	-0,5	-2,0	-1,5	58,1	58,4	59,0	-4,5	0,5	0,1	6,2	-1,2
320	-2,0	-0,6	86,1	31,7	-3,1	0,0	-1,7	1,7	58,6	58,7	59,2	-0,5	0,8	-0,2	7,0	0,0
640	-4,0	-1,0	91,2	52,9	-3,0	-2,6	-1,5	3,3	57,9	62,6	58,0	-3,4	-0,1	-2,5	8,3	-0,9

Carbon nanotubes only show limited adsorption of LDH reaching 6-8 %OD from 160 µg/mL for NM-402. LDH was not lost in tests with the other two MWCNTs.

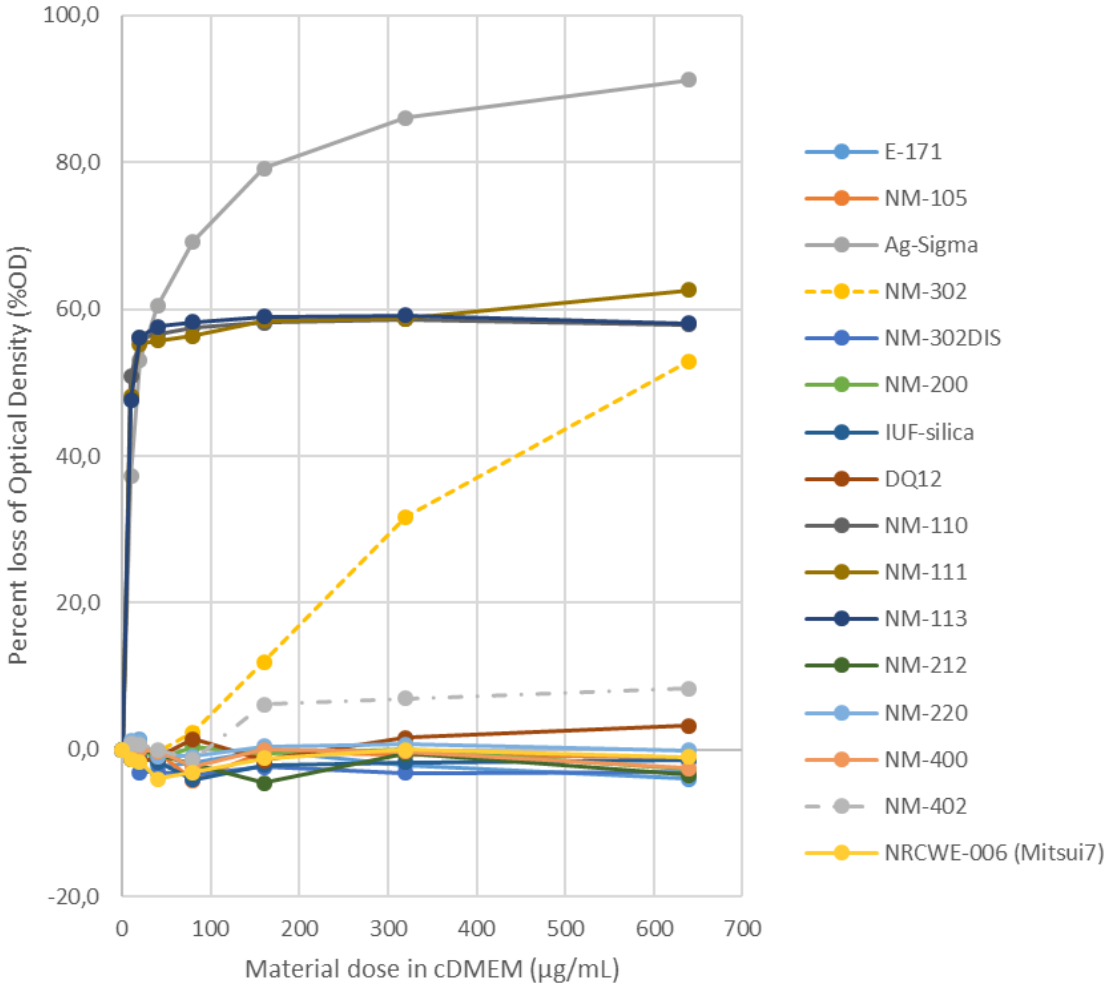

Figure 5. Percent loss of LDH as function of material dose in cDMEM calculated as relative loss of ELISA-reader optical density.

c. Pre-treatments and sequential incubation: "designed exposure identity"

When a human body takes up a particle via inhalation or oral exposure, that particle has a certain chance of being translocated to some tissue where it might induce some reaction, adaptive or adverse – but inevitably the particle will transform from the pristine physicochemical identity to the identity that acts on the tissue. At the very least, opsonins adsorb to form a corona (Monopoli et al., 2012). It has been demonstrated that some fraction of that corona is "soft", in the sense of being reversible, and another fraction is "hard", and thus a permanently adsorbed layer around the core particle (Milani et al., 2012). Here we draw the attention to "even harder" transformations that

affect the core particle throughout its journey across physiological compartments. It is evident that each compartment imposes different pH conditions, and offers reaction partners to reductive or oxidative transformation, and opsonins can favor aggregation by bridging or deagglomeration by colloidal stabilization (Figure 6). Changes may be permanent or reversible. We approach the issue by simulating the *in vivo* journey by pre-treatments that incubate the ENM in one relevant medium or sequentially in several media (up to three), before they are dosed onto the *in vitro* models. While our focus is on the particle characteristics, we also assess the ions generated by dissolution. We note that the validity of the approach is supported by OECD guidelines for the testing of non-particulate (molecularly dissolved) chemicals called “Bacterial Reverse Mutation Test”. TG471 specifies metabolization before toxicity testing. This transforms the chemical identity of the test substance through metabolization catalyzed by enzymes and co-factors to 2-50 metabolites, and thus increases the realism of the testing results. In analogy, both the particle morphology and the chemical identity of ENM may be transformed.

The concept is demonstrated on two forms of Ag ENMs, and two forms of SiO2 ENMs, both from the PATROLS Tier 1 materials. The two substances selected differ significantly in their reactivity and are meant to represent zero-valent metals and metal oxides respectively. In the recent framework by the Hurt group, they represent transformation by oxidative dissolution (Ag) and non-redox transformation (hydrolytic, acid-base) (SiO_2), respectively. (Gray, Browning et al. 2018)

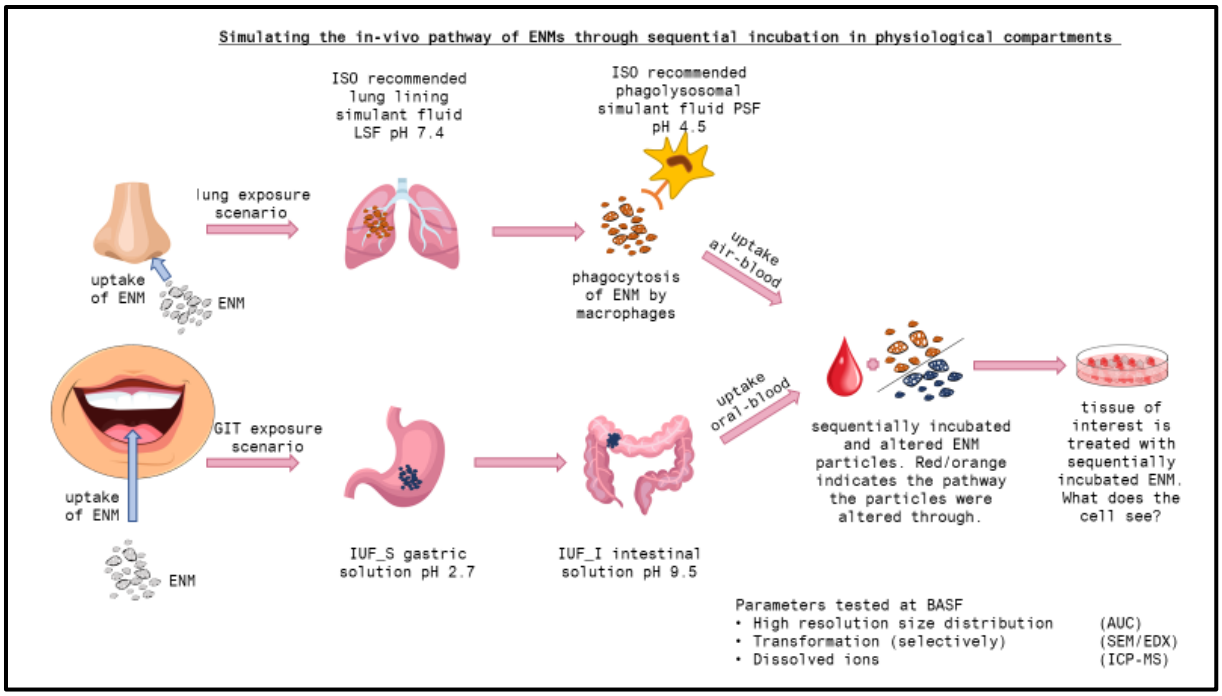

Figure 6: Pre-treatments designfor the in vitro exposure identity to better represent the identity of the particle that reaches the target tissue after a journey through several physiological compartment. The particles are incubated in up to three simulant media before they are finally dosed into cells.

Focusing first on transformation of the chemical speciation before internalisation, we analysed the particles after the IUF pre-treatment through Energy-dispersive X-ray scattering (EDXS). None of the materials showed completely unexpected signals, except for ZnO NM110 showing a significant absorption of organics with the highest nitrogen absorption (C, N ~10%). ZnO furthermore possesses the broadest size distribution indicating significant interactions which can be contributions of the positive charge. In order to zoom into the surface of the particles, where most transformation would start, we applied XPS with line shape analysis. The transformation of Ag particles before any treatment, after suspension in water with sonication, and after the IUF pre-treatment (without sonication) was measured (Figure 7). Overall the silver oxidations state varies significantly between both tested silver materials. We found Ag Sigma to truly consist of metallic silver, whereas Ag NM300 showed mostly organics (73% Carbon) and only oxidized species (Ag_2O, AgO) even before any treatment. The

predominance of organics must be attributed to the colloidal stabilisation by polymer, probably PVP, and the state of oxidation may be related to the several years of storage in the JRC repository, despite filling vials under the Argon. Triplicate measurement of Ag Sigma does not show any significant differences between the as-produced powder and the aqueous dispersion that was then dried again for XPS analysis. However, after IUF pre-treatment we observed increased amounts of Ag_2O and AgO species. This shows that the pre-treatment can induced the expected transformation by oxidative processes. In contrast, the triplicates on Ag NM300 after the IUF treatment still only expose organics with little or no detectable Ag on the surface. Such transformation would occur in the scenario of oral uptake even before the materials are internalised from the intestine to cells of the intestinal organs or to the systemic circulation. The sequential incubation to mimic physiological ADME pathways for in-vitro tests is thus especially relevant for materials that are susceptible to oxidation (such as zero-valent metals), but then should also release ions by oxidative dissolution. Dosimetry and toxicity of the ions is equally important in this case. (Gray et al., 2018).

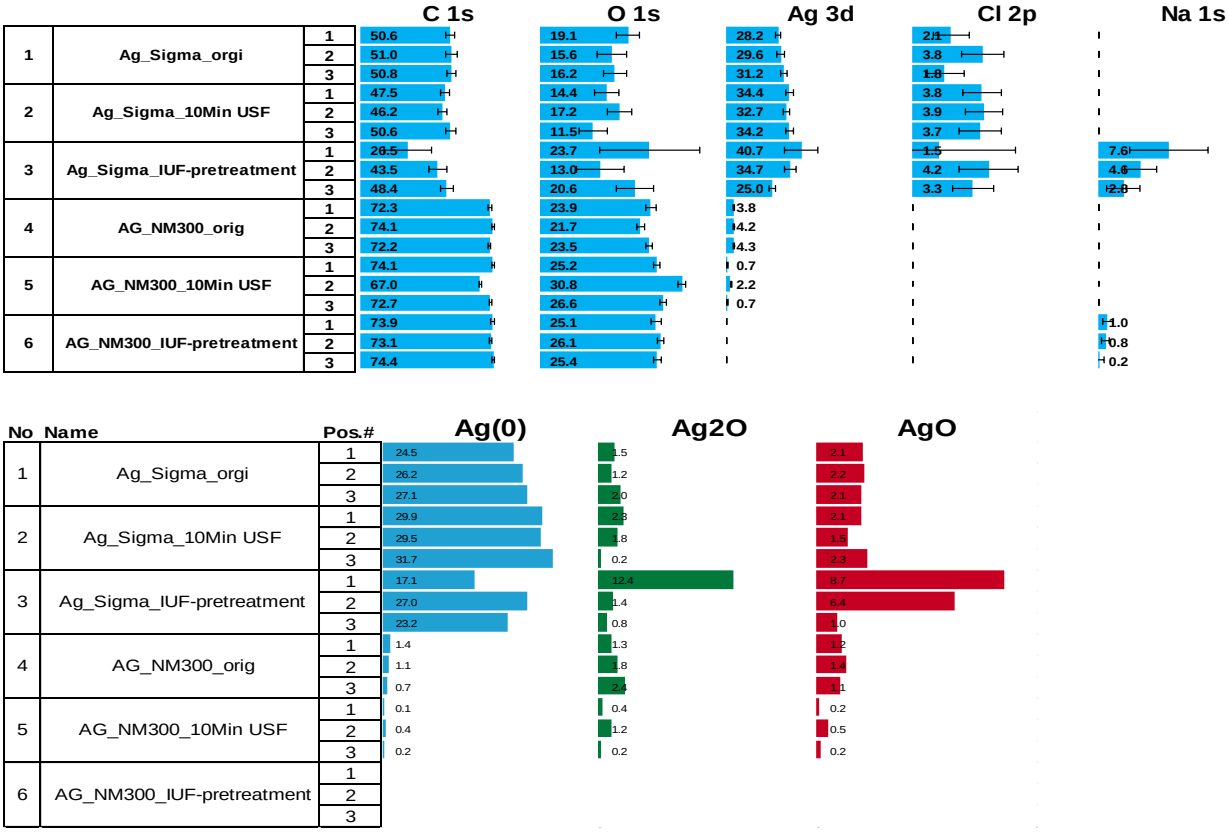

Figure 7: XPS analysis of transformation induced by the IUF (=IUF_S + IUF_I) pretreatment of the two Ag materials. As controls, the materials are analysed in the original state (no dispersion), and after dispersion in deionized water with sonication. The IUF pretreatment does not use sonication, but simulates a chemically aggressive compartment.

When measuring the ion concentration after the filtration through ICP-MS (Table 3), Ag NM300 showed no significant response to any of the single media. However, we then proceeded to simulate pathways through several compartments. Ag NM300 generated significantly more ions in the combination LSF-FBS and IUF-PSF, but not in the sequences FBS-PSF, IUF-FBS or LSF-PSF. Among these sequences, LSF-FBS simulates the pathway of passing the air-blood barrier from lining fluid to serum, and IUF-PSF simulates the passage through stomach and intestine, and uptake to lysosome, e.g. in Peyer's patches. The dissolution is not driven by a single reaction partner, because otherwise it would have occurred in the single media. Such a strong dependence on medium sequences was not observed for the other Ag nanoform.

However, the two silica nanoforms also showed increased dissolution through the LSF-FBS sequence, yet was still limited to 12 mg/L and consistent with the single media.

Table 3: Ion concentrations of Ag Sigma, Ag NM300, SiO_2 IUF and SiO_2 NM200 after filtration through a 5kDa membrane in different media. Concentrations measured through ICP-MS. The color code is normalized to maximum ion concentration per each materials.

		Ag Sigma	Ag NM300	SiO2 IUF	SiO_2 NM200
		Ion concentration [mg/L]			
Medium	FBS	0.021	0.000	4.433	5.569
	LSF	0.216	0.000	6.669	8.096
	PSF	0.000	0.353	1.532	0.598
	FBS to PSF	0.102	0.050	1.435	1.247
	IUF to FBS	0.344	0.003	1.340	4.711
	LSF to PSF	0.585	0.000	2.067	2.116
	LSF to FBS	0.392	50.751	10.730	11.506
	IUF to PSF	0.025	34.702	2.657	12.101

Apart from the chemical speciation of the particle and the release of ions, also the physical structure of particles and their agglomerates can also transform. By fractionating methods, we analysed the particle size distributions, starting from single media (Table 4). As known since the beginning of nanosafety studies, the dispersion medium has a decisive influence on the state of agglomeration of the ENM(Bihari et al., 2008; Schulze et al., 2008). The serum proteins in FBS stabilize Ag Sigma and SiO_2 NM200 better than all other media, whereas this was not observed for SiO_2 amorphous. The individual Ag NM300 particles remained stable, whereas Ag Sigma agglomerated significantly. Ag NM300 was furthermore the only ENM tested with sub 1-nm fraction. This is attributed to the generation and stabilization of Ag ions by organic complexes. Such complexes have been observed before, studying oral dissolution of Ag NM300 by Bove, Sabella et al. (Bove et al., 2017). SiO_2_amorphous

disperses to significantly smaller agglomerate sizes than SiO_2 NM200; only in PSF SiO_2 amorphous forms larger agglomerates than SiO_2 NM200. The overall variation is very low for Ag NM300 and SiO_2 NM200, but reaches a range of about 10-fold for Ag_Sigma and SiO_2_amorphous.

Table 4: Particle size distribution descriptors D10, D50 and D90 in different relevant media for Ag Sigma, Ag NM300, SiO_2 amorphous and SiO_2 NM200. The colour code is normalized to maximum diameter per each material.

		D10	D50	D90
		[nm]		
Ag Sigma	FBS	14	63	156
	IUF	47	377	704
	LSF	7	409	936
	PSF	382	545	666
Ag NM300	FBS	8	10	16
	IUF	10	12	17
	LSF	11	14	29
	PSF	10	13	24
SiO_2 amorphous	FBS	117	263	598
	IUF	57	98	167
	LSF	65	93	135
	PSF	726	1611	2200
SiO_2 NM200	FBS	273	580	1445
	IUF	499	1840	4393
	LSF	230	966	1550
	PSF	561	1194	1707

Table 5: Particle size distribution descriptors D10, D50 and D90 after sequential incubation for Ag Sigma, Ag NM300, SiO_2 amorphous and SiO_2 NM200. The code "FBS to PSF" means that the particles are first dispersed by stirring in FBS, incubated, then second medium PSF added 10:1, resuspended by sonication, incubated, then analyzed without further sample preparation directly in PSF.

		D10 nm	D50 nm	D90 nm
Ag NM300	FBS to PSF	10	12	19
	IUF to FBS	9	12	19
	LSF to PSF	10	12	19
	LSF to FBS	10	12	18
	IUF to PSF	10	12	18
Ag Sigma	FBS to PSF	6	36	115
	IUF to FBS	264	601	828
	LSF to PSF	327	603	854
	LSF to FBS	23	121	319
	IUF to PSF	264	622	952

		D10 nm	D50 nm	D90 nm
SiO2 NM200	FBS to PSF	842	1991	2670
	IUF to FBS	181	1124	1810
	LSF to PSF	654	1480	2364
	LSF to FBS	682	1541	2069
	IUF to PSF	655	1566	2566
SiO2 amorph.	FBS to PSF	308	2173	2774
	IUF to FBS	250	1248	1984
	LSF to PSF	434	1171	1686
	LSF to FBS	585	1691	2364
	IUF to PSF	486	1680	2344

By sequential incubation, we simulated the following scenarios:

- IUF_S to IUF_I (noted as „IUF“ in graphs and tables): simulates passage through gastric compartments stomach and intestine.
- IUF to FBS: simulates passage through gastric compartments, uptake through intestinal barrier into blood and systemic circulation.
- FBS to PSF: simulates systemic circulation in serum, then uptake into lysosome, e.g. by Kupffer cells in liver.
- IUF to PSF simulates passage through gastric compartments, uptake through the intestinal barrier into blood eventually uptake into lysosome, e.g. by Kupffer cells in liver. (As this already requires three sequential incubations, and considering that serum is least aggressive in comparison, we skip the intermediate incubation in FBS that would simulate the phase of systemic circulation)

- LSF to PSF: simulates alveolar deposition in lung lining fluid, then uptake by macrophages into lysosome (first step of clearance).
- LSF to FBS: simulates alveolar deposition in lung lining fluid, then uptake through air-blood-barrier into blood and systemic circulation.

We applied the same analysis as before to the size distributions after sequential incubations. The full results for two Ag and two SiO_2 materials are given in Table 5, and are plotted for one Ag and one SiO_2 material in Figure 8. The results for Ag NM300 (Figure 8_A) are easily described: this material has such a resilient colloidal stabilisation that it resists any agglomeration. The slight shift of the red dash-dotted line (incubation in FBS only) towards smaller diameters is the tell-tale signal of opsonisation (corona formation) leading to a lower effective density and thus seemingly smaller particles in the AUC technique (Walczyk et al., 2010; Wohlleben, 2012) only LSF induces minor agglomeration, but none of the sequential incubations. This is also obvious in the median D50 values in mass metrics (Table 5). As expected from its tendency to oxidize, Ag Sigma was colloidally unstable (full distributions not shown here, but median size D50 in mass metrics in Table 5).

The results are more complex for SiO_2 amorphous (Figure 8_B), but it helps to normalize the median diameter after sequential incubation by the median of the size distribution when dispersed directly into the second medium. However the size tends to remain frozen in the first medium.

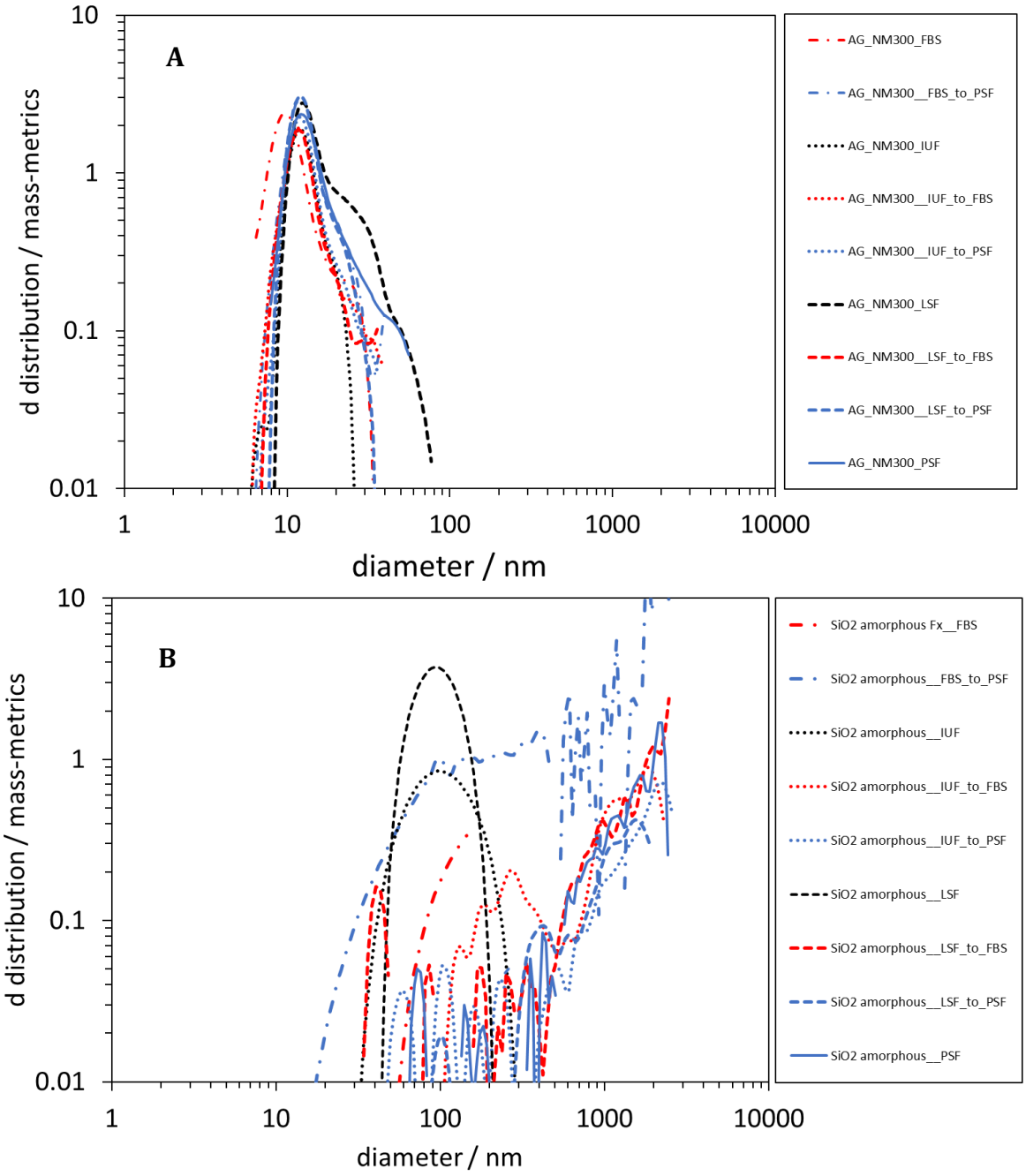

Figure 8: Particle size distribution as measured through AUC of A) Ag NM300 and B) SiO_2 amorphous after pre-treatment in different physiological media. The line type (dashed, dotted, etc.) relates to the first medium; the line color relates to the second medium. The code "FBS to PSF" means that the particles are first dispersed by stirring in FBS, incubated, then second medium PSF added 10:1, resuspended by sonication, incubated, then analyzed without further sample preparation directly in PSF.

Table 6: Particle size median (D50) after normalization to median of the size distribution when dispersed directly into the second medium. The colour code is normalized on the entire data set to highlight cases where the sequential incubation leads to very similar results (white) or lower (blue) or higher (red) agglomeration as compared to single incubation in either the first or the second medium of the sequence.

		relative to 1st medium	relative to 2nd medium
Ag NM300	FBS to PSF	120%	92%
	IUF to FBS	100%	120%
	LSF to PSF	86%	92%
	LSF to FBS	86%	120%
	IUF to PSF	100%	92%

		relative to 1st medium	relative to 2nd medium
SiO_2 NM200	FBS to PSF	343%	167%
	IUF to FBS	61%	194%
	LSF to PSF	153%	124%
	LSF to FBS	160%	266%
	IUF to PSF	85%	131%

Ag Sigma	FBS to PSF	57%	7%
	IUF to FBS	159%	954%
	LSF to PSF	147%	111%
	LSF to FBS	30%	192%
	IUF to PSF	165%	114%

SiO_2 amorph	FBS to PSF	826%	135%
	IUF to FBS	1273%	475%
	LSF to PSF	1259%	73%
	LSF to FBS	1818%	643%
	IUF to PSF	1714%	104%

The normalisation evidences that for SiO_2 amorphous the state of agglomeration after sequential incubation is very similar to the agglomeration created by dispersing directly into the second medium (white colour code in comparison to second medium in Table 6). The same is observed for the SiO_2 NM200 material. This means that for a metal oxide, with limited options of chemical transformation, the sequential incubation is an unnecessary complication of the sample preparation, because it leaves little traces on the material. The same result would be obtained by directly dispersing the material into the medium that is relevant to the cells.

In contrast, a reactive material such as Ag Sigma shows large differences by sequential incubation as compared to single media (blue and red colour codes in Table 6). It actually tends to remain frozen in the state of agglomeration induced by the first medium (more intense colours in comparison to second medium than comparison to first medium in Table 6). This means that for a reactive material, the exposure identity

is formed by the pre-treatments, which are a means to design "what" is exposed onto the cells. However, even for Ag this cannot be generalised: the counterexample is Ag NM300, which is chemical oxidised already and colloidal stabilized by polymers, such that only the release of ions leaves a trace of the pathway of compartments that was simulated.

However, the effects observed may be a trivial result of prolonged incubation. To check this hypothesis, we performed the sequential incubation protocol with one and the same medium. We selected the most labile (most reactive) material for this test, Ag_Sigma. Table 7 assembles the results obtained. The comparison of sequential incubation vs. same-same incubation shows that it is not the *length* of incubation, and not a single *medium*, but indeed the *sequence* that is decisive for the final size of Ag_Sigma:

- PSF to PSF is markedly different from FBS to PSF (numbers in brown).
- IUF to IUF is markedly different from IUF to FBS (numbers in red).
- LSF to LSF is markedly different from LSF to FBS (numbers in grey).

Table 7: Particle size median (D50) after normalization to median of the size distribution when dispersed directly into the second medium. The colour code of the NUMBERS identified values that should be compared to each other. The colour code of the CELLS is normalized on the entire data set to highlight cases where the sequential incubation leads to results very similar (white) or lower (blue) or higher (red) agglomeration as compared to single incubation in either the first or the

		relative to 1st medium	relative to 2nd medium
Ag Sigma	FBS to PSF	57%	7%
	IUF to FBS	159%	954%
	LSF to PSF	147%	111%
	LSF to FBS	30%	192%
	IUF to PSF	165%	114%
	IUF to IUF		149%
	LSF to LSF		100%
	PSF to PSF		128%

second medium of the sequence.

In summary, we recommend that sequential incubations are not performed routinely. We provided evidence that on a metal oxide the influence on the exposure identity are marginal. A framework of transformation and reactivity, such as the scheme by Gray et al.(Gray et al., 2018) can be used to predict which material is sufficiently susceptible to transformation. By this rationale, zero-valent metals are especially susceptible to non-reversible transformation. For materials susceptible to transformation, the increased sources of error by multiple pre-treatments are overcompensated by the increased realism of the exposure identity.

2.1 "How much" of the dose is effectively delivered

a. *Approaches to the effective dose by DG modelling*

Adequate dose metrics are an essential part of PATROLS strategy towards the development of alternative testing methods that investigate the hazard potential of ENMs, based around specific design requirements. The first one is that they must deliver valid predictions as compared against established regulatory tests; second, they should be more robust, simpler and less expensive than current methods. Third, due to the large number of ENMs that need to be tested, it becomes strategic to test samples in parallel, and thus supporting the throughput analysis. A freeze-thaw protocol fulfils these requirements. Freeze-thawing would enable samples prepared by the NANoREG sample preparation protocol with extended sonication to be run in parallel, which is more efficient than running multiple sonication, dynamic light scattering (DLS) and effective dose setups in parallel. In a recent publication by Vila et al.(Vila et al., 2017), a freeze-thaw protocol to enable the parallel testing of different ENMs was introduced, but further research is needed to explore variations in the effective density and dosimetry measurements with the new freeze-thaw protocol.

The goal of dosimetry modelling is to use physicochemical characteristics to predict the number of particles that come in touch with cells in an *in silico* setting. In *in vitro* settings, ENMs can have significant interactions with biological media, unlike what is observed in small molecule-based systems. Unique ENM behaviours include the formation of a protein corona as well as particle dissolution, leading to changing settling and diffusion profiles. The properties of these ENM behaviours are dependent on environmental factors such as temperature, media composition, media viscosity and pH. A model which considers the different physical theories that govern diffusion and sedimentation, and allows for complex data inputs such as size distributions and effective densities, would give a toxicologist with access to a characterization library the ability to consider ENM complexity allowing them to design experiments that produce relevant, accurate, and translatable results. These type of *in vitro* dosimetry models have been under development for the past decade, with the field advanced greatly by the work of the Teeguarden and the Demokritou groups, who developed the In vitro Sedimentation, Diffusion and Dosimetry (ISSD) and Distorted Grid (DG) models of *in vitro* nanomaterial dosimetry, respectively(Cohen et al., 2014; DeLoid et al., 2017, 2015; Lison et al., 2008; Teeguarden et al., 2007). The DG model is an advanced MATLAB-based model that considers additional variables, such as size distribution, as well as different behaviours and boundary conditions, such as diffusion, sticky and non-sticky bottoms, particle size distributions and effective density.

With this aim in mind, we have built a characterization library that can associate the physicochemical characteristics of ENMs to their behaviour in physiological media, which can then be used to accurately model *in silico* how the materials will behave *in vitro.* These results can then guide the decision of whether a particular ENM needs additional testing *in vivo*. As part of the characterization library, we also explored the sensitivity of the predicted deposited dose as modelled by the DG model to several

parameters such as: the sample preparation, adoption or not of freeze-thawing protocol and variability between triplicates, thermodynamic boundary conditions such as the stickiness of the bottom of the wells, and the particle size distribution measurements, as derived by the comparison of different techniques.

EFFECTS OF FREEZE-THAWING TREATMENT

In Table 8, a full set of experimental data, referred to freeze-thawed suspensions and used as inputs for DG model, are reported. In order to test the suitability of the freeze-thawing preparation option, in Table 9 we report the DLS mean size diameter (Z-average) and VCM effective density of fresh and freeze-thawed suspensions, comparing different media such as water + BSA (stock), DMEM/FBS and RPMI media. Here we observed relatively small differences in Z-averages of stocks (fresh vs freeze-thaw), below 30%. Note that these discrepancies contrast the claims made by Vila et al (Vila et al., 2017), which found no differences between flash-frozen and fresh samples. We also evaluated the differences in Z-average of NPs dispersed in two different media DMEM/FBS and RPMI. The data clearly shows that the difference between fresh and freeze-thawed suspension is more significant for RPMI than for DMEM/FBS. In particular, significant differences between fresh and freeze-thawed samples were found for CeO_2 NM-212 and amorphous SiO_2, whilst differences for $BaSO_4$ stay below 10%. Surprisingly, we found that effective density is much more resistant to freezing induced changes than DLS-size and found no significant differences between fresh and flash-frozen samples. Being highly probable that freeze-thawing methods will continue to be used within industrial applications, as it saves time by a factor of 2x, we should take into consideration, potential variations deriving from freeze-thawing treatment, that, despite the use of identical standardized dispersion protocol, could justify discrepancies between *in silico* modelling and *in vitro* toxicology.

Table 8: DLS hydrodynamic diameter size (Z-Average) and effective density of primary dispersion (stock) and after 1-hour incubation in complete DMEM/FBS.

ENM	Z-Average (nm ± σ)		Effective Density (g/cm^3 ± σ)
	Stock	DMEM/FBS	DMEM/FBS
TiO_2 NM-105	274.9±46.4	287.7±42.8	1.408±0.009
CeO_2 NM-212	281.0±18.9*	242.6±2.6*	2.214±0.029
$BaSO_4$ NM-220	176.4±37.9	151.1±27.5	2.034±0.049
Ag NM-300K	135.1±3.8	92.7±14.7	2.004±0.153
Ag NM-302	1104.0±114.6	1027.4±44.0	8.617±0.181
SiO2_amorphous	230.8±26.8	1169.1±155.2	1.156±0.013
Ag Sigma	195.1±5.5	163.0±2.7	2.465±0.093
SiO_2 DQ12	471.0±19.7	402.4±44.1	1.787±0.000

Table 9: Comparison of Z-Average and effective density of fresh (FR) and freeze-thawed (FT) suspensions in DMEM/FBS and RPMI.

ENM	Z-Average (nm ± σ)						Effective Density (g/cm^3 ± σ)		Deposited Dose*		
	Stock		DMEM/FBS		RPMI						
	FR	FT	FR	FT	FR	FT	FR	FT	FR	FT	D
NM 212	219 ±2	281 ±18	261 ±4	243 ±3	339 ±6	655 ±58	2.200 ±1	2.214 ±1	16.5	44.3	27.9
NM 220	126 ±1	176 ±37	116 ±2	151 ±27	172 ±7	199 ±2	2.174 ±1	2.034 ±1	3.1	9.0	6.0
SiO_2 IUF	148 ±1	231 ±26	1161 ±72	1169 ±155	225 ±4	421 ±25	1.156 ±1	1.156 ±1	87.9	73.5	14.4

*% at bottom of well after 24hrs, Initial Concentration: 0.256 mg/mL, reflective boundary conditions

In order to deeply investigate how the observed physiochemical changes would affect dosimetry, the deposition of particles with and without freeze-thawing treatment was modelled using the DG model, as described in the method section. The deposited dose after 24 h was modelled for certain ENMs at a concentration of 0.0256 mg/mL, with

reflective boundary conditions. We compared fresh and freeze-thawed suspensions of three ENMs: CeO_2 NM-212, $BaSO_4$ NM-220 and SiO_2 Amorphous. Despite to slight differences in the Z-averages between fresh and flash frozen samples (both for stock and incubated samples, Table 9) the differences in the fraction deposited dose were evident (Figure 9). The sedimentation rate of freeze-thawed samples was higher for $BaSO_4$ NM220, CeO_2 NM212 and lower for SiO_2 amorphous. These differences could be justified by the difference in particle size distribution shown in Figure 10, even if no clear trend and correlation have been identified. The main effect seen in some materials, such as CeO_2 NM-212, was a small increase in the overall radii, whilst other materials showed a developed a multimodal size distribution. As can be seen in Table 9, the change in particle size distributions translated to large differences in some of the materials, with an increases of DLS mean diameter of 61.7 nm, 50.3 nm and 82.5 nm for CeO2 NM-212, BaSO4 NM-220 and Amorphous SiO2, respectively, if compared fresh and freeze-thawed stocks.

EFFECTS OF VARIABILITY BETWEEN TRIPLICATES

The robustness of DG model was also tested considering the variability between different suspensions of the same material. Depending on the material analysed it was found that only CeO_2 NM-212 showed large variability in percent-deposited after 24 hours (Figure 9A), other materials, such as NM-220 and Sigma Ag, showed much less variability, in the range of 7-14% (Figure 9B and 9C). The particle size distribution for unfiltered samples as measured through DLS is prone to be affected by small numbers of large agglomerates within the dispersion. As seen in Figure 9, Ag Sigma was the only material to give a good reproducibility among three triplicates. The differences between Triplicate 1, and Triplicates 2 and 3 for CeO_2 NM-212 are most likely due to a poor dispersion of Triplicate 1. A sample that is not correctly dispersed can result in a different deposition profile after modelling. While sample to sample variability is to be

expected, these simulations highlight the concern that variability may be propagated and multiplied during experiments that rely on multiple dependent measurements. This type of error propagation can be calculated using accepted statistical tools. It is thus key for future experiments to investigate whether averaging n number of dispersions, and subsequent characterization, will result in sufficiently accurate dosimetry data for biological experiments. These future experiments may focus on quantitatively measuring deposition in a controlled environment and comparing the measured deposited fraction to that predicted by simulations using averaged characterization data. The experiment itself might look like those conducted(DeLoid et al., 2015), or an alternative method. Ideally, these experiments will reveal the required number of replicates for materials to result in an average that, when modelled, will reflect reality.

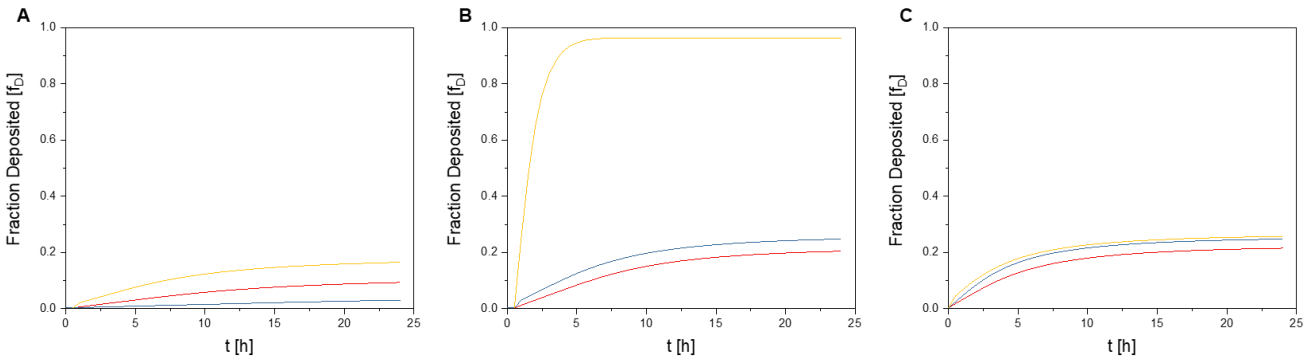

Figure 9: Fraction deposited dose vs samples preparation variability: A $BaSO_4$ NM-220, B CeO_2 NM-212 and C Sigma Ag. The model was set up to use the apporpriate variables for each material, with the only difference between each simulation being a different nanoparticle size distribution, as aquired by DLS, and different effective densities, measured using VCM. The three different colors are representing the different runs.

EFFECTS OF DIFFERENT THERMODYNAMIC BOUNDARY CONDITIONS (STICKINESS)

Finally, we tested how the DG model is affected by thermodynamic boundary conditions. The DG model has built into it the capability to simulate different levels of "stickiness" between nanoparticles and the bottom of the well. Varying stickiness allows the model to account for the different ENM uptake rates based upon cell type. The method used to model this stickiness is described in the original publication for the

DG model. Briefly, stickiness is simulated using a Langmuir-isotherm adsorption process, where the particles are adsorbed and desorbed to the bottom of the well. Once adsorbed, the particles are removed from the system until desorbed. Once the stickiness is included, it is defined by ascribing an association constant, Kd, to the NPs. Kd is assumed to be specific to each experimental condition and is not well understood, but it is thought to be cell-, ENM-, and media-dependent. We studied what effect this addition to the simulation would have on data collected, and how significantly stickiness would affect dosimetry based upon experimental data. We simulated dosimetry in the DG model, with the boundary being either reflective (adsorption turned off), low-adhesion (Kd = $1x10^{-8}$), or high-adhesion (Kd = $1x10^{-9}$). The Kd values were chosen following the work originally done by DeLoid et al. (DeLoid et al., 2015). We examined this by modelling deposition over 24 hours in three materials: A $BaSO_4$ NM-220, B, CeO_2 NM-212 and C Ag Sigma (Figure 10). It was found that the different boundary conditions can significantly affect dosimetry in a material-dependent manner, with higher simulated adhesion leading to higher particle sedimentation rate. DG model also showed a strong dependency on further parameters such as the simulation of the height of the sub-compartment. When using 0.01 mm, the suggested height of the sub-compartment, we interestingly observed some major dips within the curve of the deposited dose over time (Figure 11). When adjusting this height of the sub-compartment to 0.0005 mm, the dips vanish, however, the time for modelling the dosimetry changes from a few hours to several days. Furthermore, the adjustment of the adhesive boundary has a major effect on the deposited dose with the boundary being either reflective (adsorption turned off), with low-adhesion (Kd = $1x10^{-8}$), or high-adhesion (Kd = $1x10^{-9}$). The resulting dosimetry curves behave mainly as expected, with higher deposited doses in high-adhesion conditions compared to the other conditions. The measurement of the deposited dose exhibits a sensitivity towards

different ENM substances, such as the Ag NM300k as well as the SiO_2 amorphous nanoform. The results obtained by choosing the adhesive boundary are not affected by sedimentation of small particles with diffusion driven sedimentation.

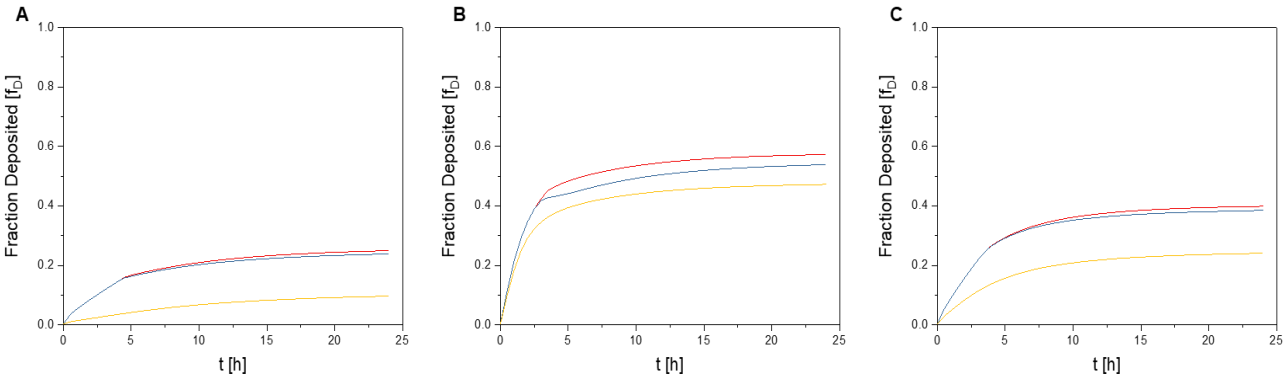

Figure 10: Fraction deposited dose vs assumptions on boundary conditions: A $BaSO_4$ NM-220, B CeO_2 NM-212 and C Sigma Ag. The red curves correspond to a K_d (M)=1x10^9, blue corresponds to K_d (M)=1x10^8 and the yellow curve corresponds to no boundary conditions, resulting in a reflective bottom.

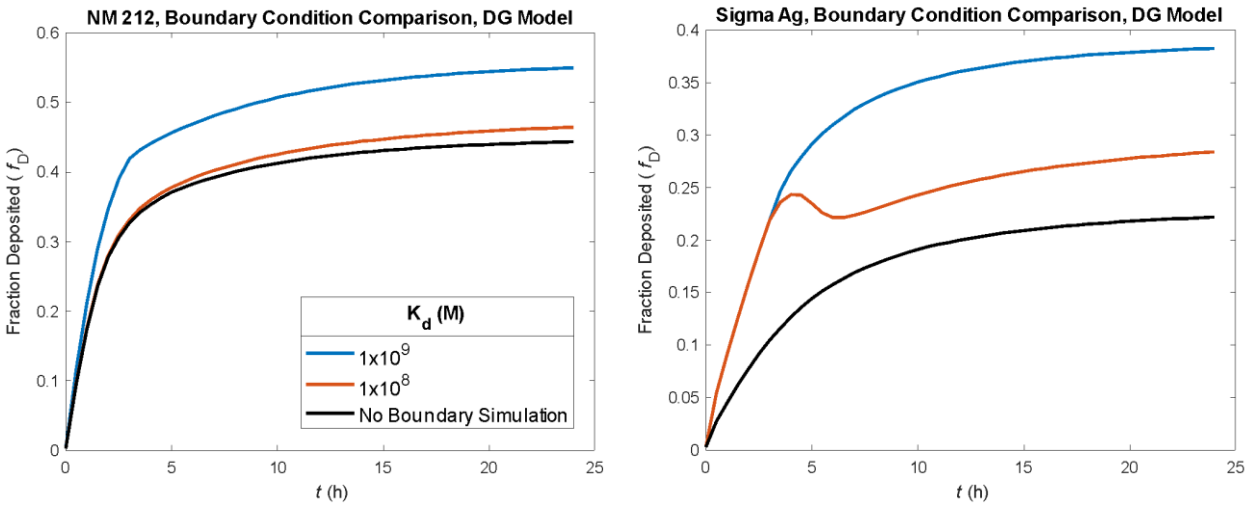

Figure 11 Comparison of boundary conditions for A CeO_2 NM-212 and B Ag Sigma with bad input parameter as seen in dent in red curve for Ag Sigma.

EFFECTS OF DIFFERENT METHODS USED TO PROVIDE SIZE DISTRIBUTION

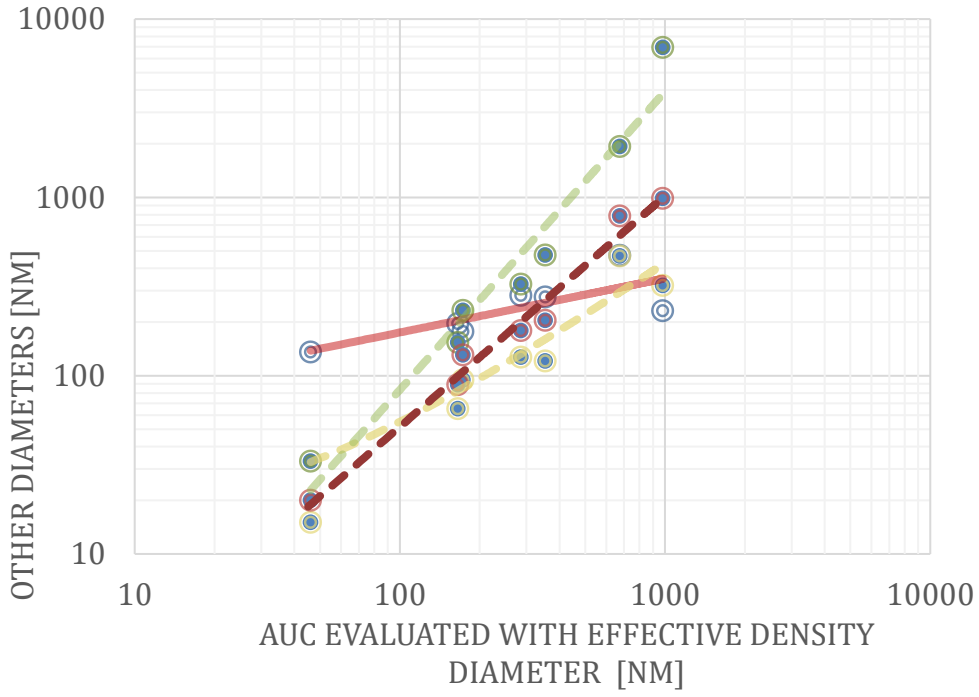

Figure 12: Parity plot of the mass median particle diameter with different density assumptions for AUC and DLS measurements for SiO_2 amorphous, SiO_2 DQ12, TiO_2 NM105, CeO_2 NM212, $BaSO_4$ NM220, Ag NM300K and Ag Sigma. The solid red line corresponds to the DLS measurement. The red dashed line connecting the blue dots with red outer shell corresponds to the AUC fractal dimension evaluation with D=2.54. The green dashed line connecting the blue dots with green outer shell corresponds to the AUC fractal dimension evaluation with D=2.1. The yellow dashed line connects the blue points with the yellow sphere and describes the AUC solid sphere evaluation with D=3. Linear regression was used for the fits in the double log plot.

Since the measured polydispersity of the size distribution was found to be critical for the DG predictions, we explored the model's sensitivity to different methods of determining the size distribution. DLS is known to be very reliable on the Z-average diameter, but less so on the complete distribution. Fractionating methods instead have the advantage of quantification of a few-percentage fractions of agglomerates, or of individual constituent particles. Here we compare DLS to AUC size distributions, evaluated with the independently measured effective density, and find that the parity plot between AUC and DLS has a slope far below parity, indicating that the DLS

differentiates the median size between different ENMs to a far lesser extent than AUC (Figure 12).

We so employed the size distributions from DLS and AUC in the DG model to derive the deposited dose (Table 10) and found significant differences that can be related to the differences in PSD.

Table 10: Fraction Deposited after 24 hours (%).

	DG prediction,			**Measured (sedimentation transport only)**
	DLS input, Reflective Boundary	DLS input, Adhesive Boundary (K_d=1x10^{-9} M)	AUC input, Adhesive Boundary (K_d=1x10^{-9} M)	Sedimented dose measured directly from the S_{ved} values as received by AUC-measurements
	[% deposited dose after 24h]			
SiO_2 amorphous (IUF)	73.57	74.77	56.0	60.50
SiO_2 DQ12	49.02	60.64	30.88	68.67
TiO_2 NM-105	18.53	25.69	20.80	42.67
CeO_2 NM-212	44.33	54.97	40.98	42.00
$BaSO_4$ NM-220	9.05	23.67	1.9	15.33
Ag NM-300K	31.93	41.81	17.02	-
Ag Sigma	22.17	38.25	3.74	14.67

The significant impact of using the particle size distribution from two different characterization techniques to model the deposited dose was recently described by(Petersen et al., 2019). Petersen demonstrates that using the mean diameter instead of the PSD does not strongly affect the calculation of deposited dose (differences below 10%), whereas using substantially different analytical techniques for the determination of the PSD can in some cases yield substantially different modelled concentrations that reaches the cells, thus potentially altering interpretations of the dose-response, due to the presence of tails toward smaller or larger sizes. Finally, we compared two methods to determine the deposited dose, the DG prediction with AUC integration of sedimentation coefficients as measured experimentally. The two methods differ in their principle of particle transport. AUC only takes sedimentation

into account, whereas DG uses both diffusion and sedimentation. As shown in Table 10 the deposited dose modelled by the DG model with DLS as input data for the particle size distribution, matches the deposited dose as calculated by AUC directly quite well, whereas the DG model using AUC size distribution data differs overall by more than 30%.

Furthermore, when comparing the modelled deposited dose to the sedimented dose measured directly from the S_{ved} values as received by AUC-measurements, the direct comparison of predicted deposited dose to AUC measurements (under accelerated gravitational forces, thus suppressing the diffusional contribution) shows good

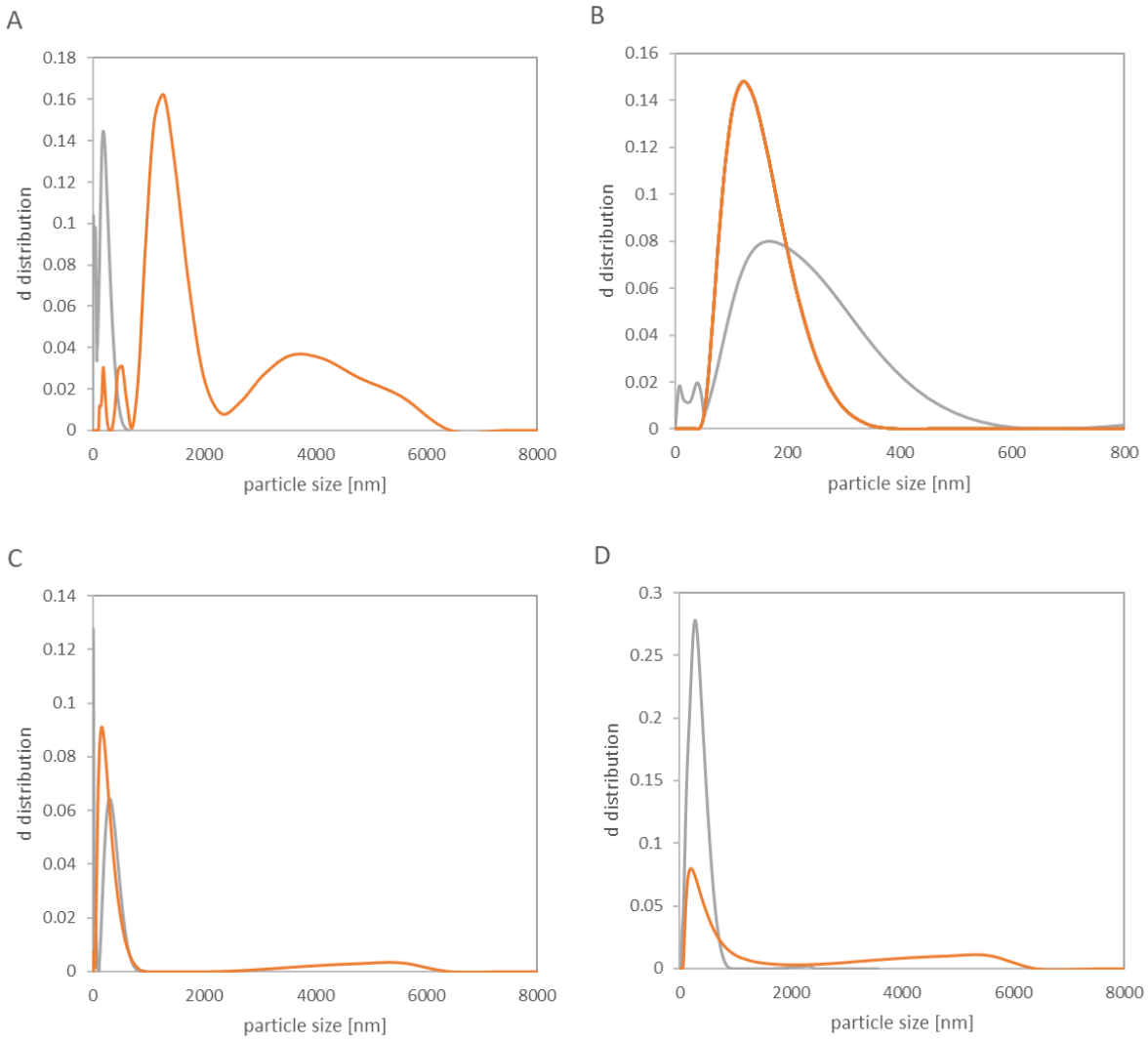

Figure 13 Particle size distribution for A SiO_2 Amorphous, B Ag NM300K, C $BaSO_4$ NM-220 and D CeO_2 NM-212 as measured by DLS (orange) and AUC (grey) with fractal dimension evaluation Df=2.54.

agreement for SiO_2 amorphous and $BaSO_4$ NM-220, for which sedimentation is the dominant transport, whereas the discrepancy is significant for SiO_2 DQ12 and Ag NM-300K, for which diffusion dominates the transport (Figure 13). This is consistent with the relatively narrow size distribution of SiO_2 DQ12 and Ag NM-300K at smaller sizes. We had expected that the deposited dose for DG modelling should at least be as high as the deposited dose directly obtained through measuring the sedimentation by AUC, but did not find that to be the case, even when using AUC size distributions as DG input.

Through previous modelling with the in vitro sedimentation, diffusion and dosimetry (ISDD) model it was observed that for agglomerated particles the predictability of deposited dose is low whereas well dispersed single particles tend to have a higher deposited dose.

Modelling Consistency.

Our complementary data by hydrodynamic characterisation with VCM, DLS or AUC input can finally be interpreted in terms of the hydrodynamic properties of ENM-protein structures. DeLoid *et al* highlighted that the concept of effective density is related via the Stirling formula to the fractal dimension of ENM agglomerate(Cohen et al., 2014). An existing implementation of fractal dimensions in AUC (Wohlleben, 2012) can be used to match the fractal dimension in the Stirling formula such that the median diameters agree with the evaluation by the measured effective density. Evaluation with D_f=3 (corresponding to solid spheres) remains *below* parity suggesting D_f=3, but also the expectation from the theory of reaction-limited colloidal aggregation (RLCA)(Lin et al., 1990) does not fit, because the evaluation with D_f=2.1 remains *above* parity. The best approximation to parity is reached by D_f=2.54. This value is nearly identical to the theoretical expectation for diffusion-limited colloidal aggregation (DLCA).(Lin et al., 1990). We can thus interpret that the ENM-protein agglomerates assemble with a high

stickiness (hence DLCA) upon each collision of ENMs with their protein corona.

Conclusion

We explored the sample preparation and the dosimetry of ENM *in vitro* testing. Regarding the sample preparation, the freeze-thaw protocol enables parallel testing by flash freezing the samples after sonication; this does alter the particle size distribution, of fresh dispersions up to 35% however after one-hour incubation the difference is below 25%. The effective density is only altered by +-0.15 g/cm^2. Thus, overall it modulates the dosimetry of the particles. The modulation tends to be lower in DMEM/FBS than in RPMI without serum. Nevertheless, the key for relevant results which is the consistency between characterization *in silico* modelling, and *in vitro* toxicology can be obtained.

Regarding dosimetry, the fundamental notion that the deposited dose is lower than the total administered dose can be easily supported by simple measurements (DLS, VCM) and DG modelling. With a deposited dose ranging between 9-73% for the different ENMs with reflective boundary conditions, we observe that the prediction of deposited dose varies significantly. However, the uncertainty of the actual deposited dose is considerable. Especially when using standardised dispersion protocols (NANoREG) and/or polydisperse industrially relevant materials, the predictions of the model incur an uncertainty of the deposited dose based upon uncertainty in the inputs. The dose-response that is obtained by the modelled prediction of deposited dose can thus shift. If the *in vitro* reactivity of different nanoforms differs by the same factor as the input uncertainty, we cannot conclude if the results are from a similarity of biological interactions or methodical uncertainty of the modelling.

Especially for well-dispersed ENMs, uncertainty is introduced by choosing an arbitrary choice of affinity of particles to cells (“reflective” vs. “adhesive” bottom). Additionally, for polydisperse ENMs, minor details of the particle size distribution strongly influence

the modelled dosimetry, such that the choice of the measurement technique -e.g. DLS or AUC introduces further uncertainties to the dosimetry modelling. For any polydisperse ENM, we found it necessary to increase the DG model computing resources by reducing the output compartment height to 0.0005 mm; otherwise, dips in the particle settling traces lead to erroneous predictions.

b. *Experimental validation of DG dosimetry model*

INTRODUCTION

The aim of this study was to support and validate the DG model developed and applied to passive and active NPs (MG3 and MG4 from D4nanoGrouping) in biological toxicological relevant medium, milli-Q water plus 10% fetal bovine serium (FBS) (Arts et al., 2016). The study described the colloidal behaviour and sedimentation kinetic in 24 hours for $BaSO_4$ (NM-220), CeO_2 (NM-212) and TiO_2 (NM-105) at half height of the a cylindric experimental set-up. This system was designed and developed to reproduce the well plate conditions of in-vitro tests and a layer of gelatine+ GPTMS on the bottom of the experimental set-up was deposited to mimic the NPs cell uptake.

We proceeded with colloidal behaviour and sedimentation kinetic evaluation, considering DLS/ELS and ICP-OES measurements at half height of the water column for $BaSO_4$, CeO_2 and TiO_2 NPs.

$BaSO_4$

The hydrodynamic diameter values do not present a trend with high polydispersity, without being affected by exposure time, and size values that increase only in function of increase in NPs content (Figure 14).

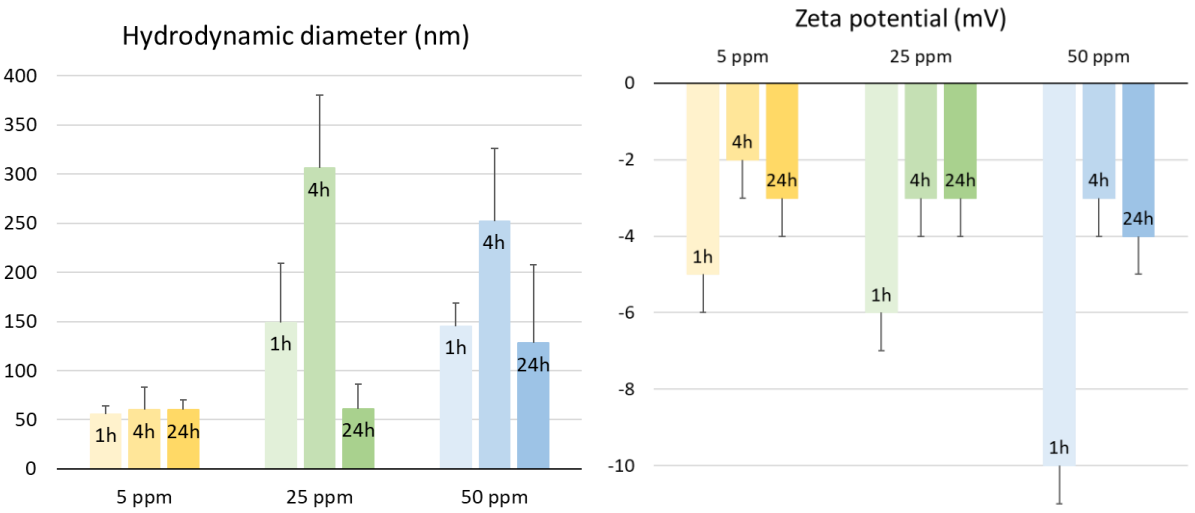

Figure 14: DLS (left) and ELS (right) measurements at half height of 5, 25 and 50 mgL^{-1}, $BaSO_4$ samples after 1, 4 and 24 h of incubation.

While absolute ZP values decrease in time for all concentration, suggesting a destabilization in time of the nano-suspensions. In the sedimentation kinetic referred at half height of the water-column, the results show that in samples more concentrated the progress of agglomeration and precipitation vs time of exposure, occur with higher intensity, most evident for sample at 50 mg L^{-1} (Figure 15).

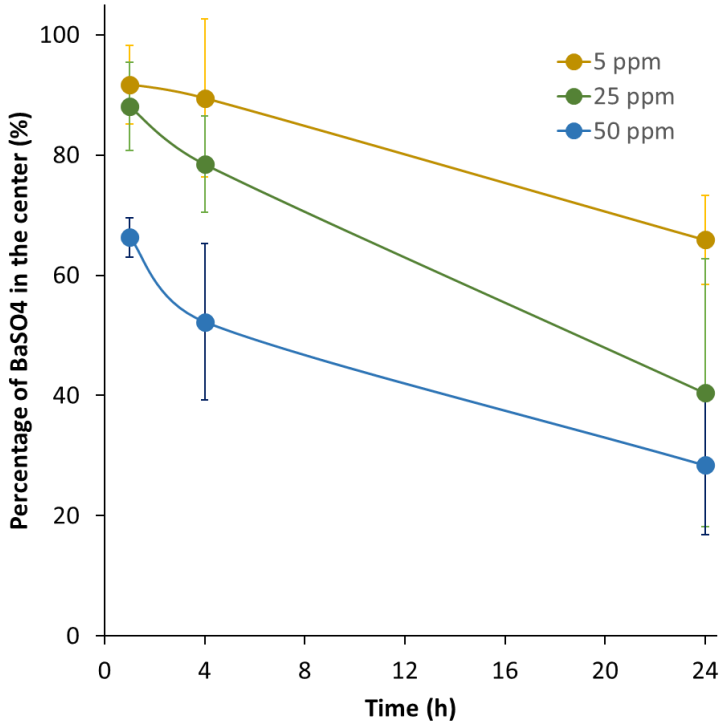

Figure 15: $BaSO_4$ NPs concentration (%) at half height of water column for 5, 25 and 50 mg L^{-1} samples

as a function of time (1, 4 and 24 h).

CeO_2

At low concentrations (5 and 25 mg L^{-1}), the size distribution present similar values with high polydispersity at all exposure times, just slightly increasing from 5 mg L^{-1} to 25 mg L^{-1} (from ca. 250 nm to 350 nm). While in the 50 mg L^{-1} sample, we noticed an increase in size dimension in time, probably associated with the agglomeration process, and more evident at the highest concentration (Figure 16). ZP values tend to decrease from absolute values at higher exposure times, halving the 1h value after 24h. The exception is the 25 mg L^{-1} sample, where ZP values are the same after 1h and 24h of exposure (Figure 16). Looking at NPs concentration (%) at half height of water column, there is a decrease in the concentration as a function of time, but not as a function concentration (Figure 17). This behaviour could be associated with a stabilization of NPs by FBS presence, that acts as surfactant and provide similar data for all concentrations.

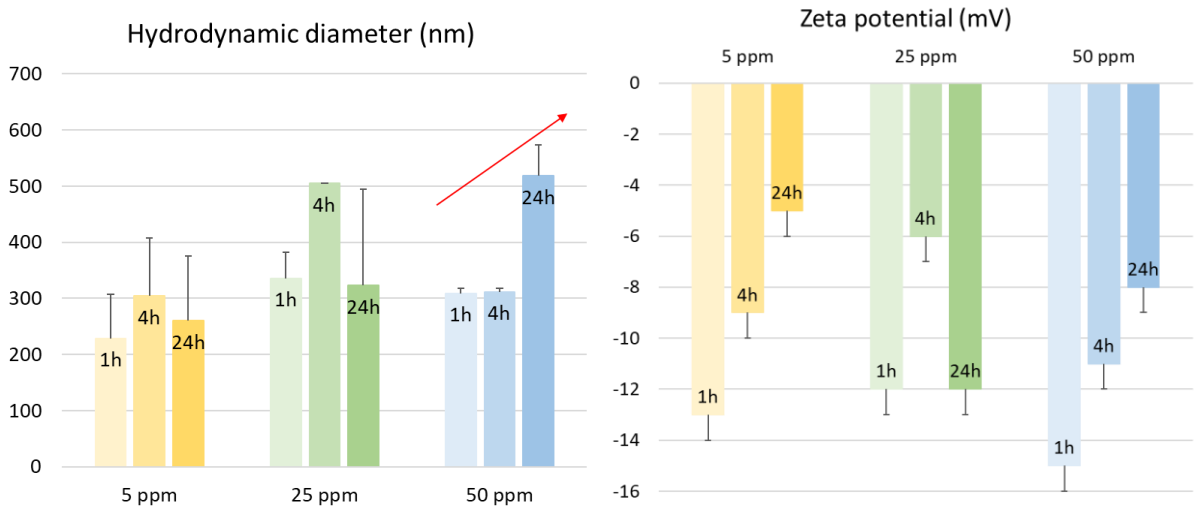

Figure 16: DLS (left) and ELS (right) measurements at half height of 5, 25 and 50 mgL^{-1} CeO_2 samples after 1, 4 and 24 h of incubation.

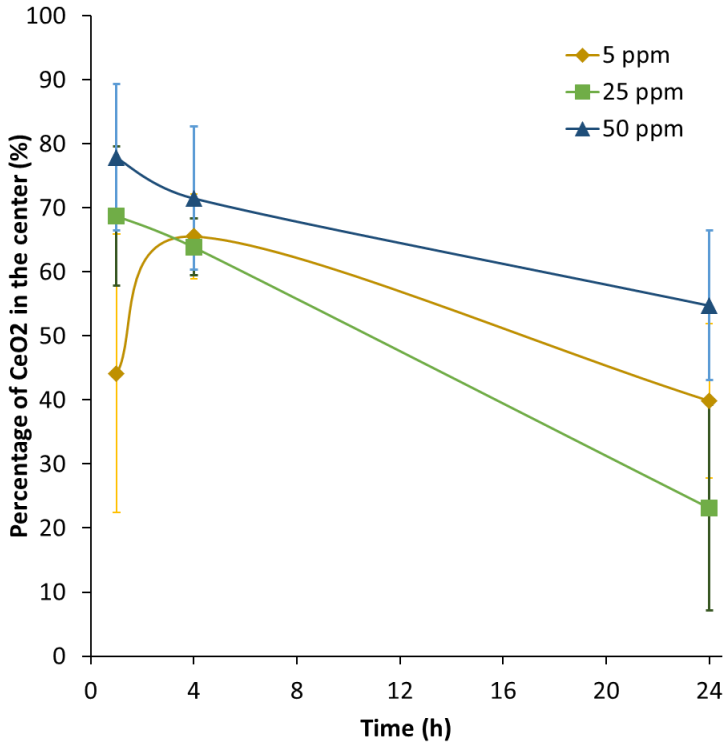

Figure 17: CeO_2 NPs concentration (%) at half height of water column for 5, 25 and 50 mg L^{-1} samples as a function of time (1, 4 and 24 h).

TiO_2

TiO_2 NPs, as CeO_2 NPs, at low concentration (5 and 25 mg L^{-1}), presents similar values of size, with high polydispersity at all exposure times. A different situation occurs in the 50 mg L^{-1} sample, where we noticed a decrease in size dimension in time, probably associated with medium interaction (Figure 18). As for all the other NPs, also in TiO_2 samples ZP values tend to decrease from absolute values at higher exposure times, halving the 1h value after 24h in the 5 and 25 mg L^{-1} samples. The exception is the 50 mg L^{-1} sample, where ZP present almost stable values after 1h and 24h of exposure (Figure 18). At half height of the water column, the decrease in NPs concentration (%) is a function of time, but not as a function concentration, where the most stable sample is the most concentrated (Figure 19). This behaviour could be associated with NPs stabilization by the presence of FBS, that acts as surfactant and results in similar data for all concentrations.

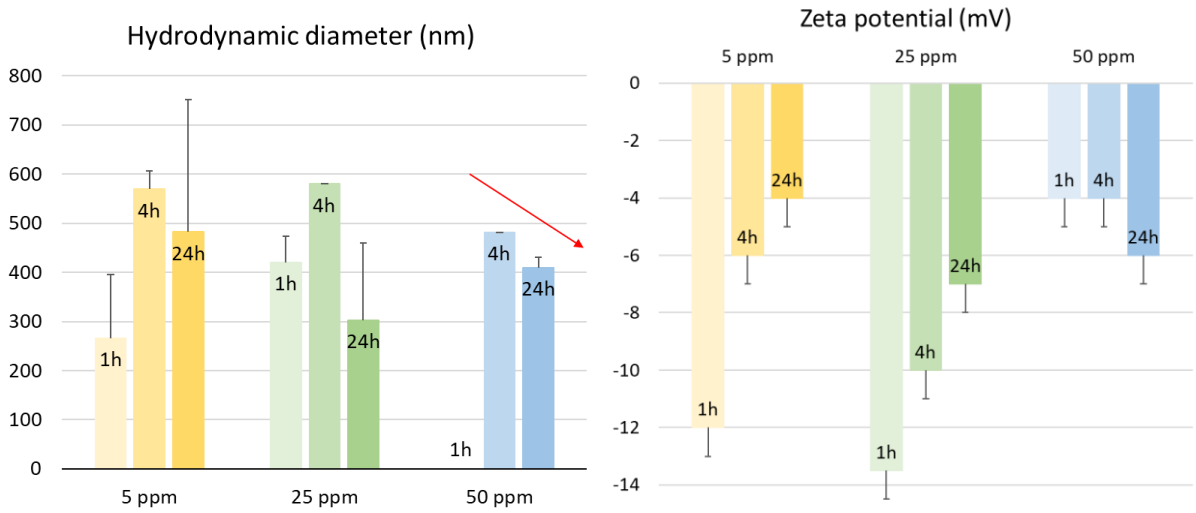

Figure 18: DLS (left) and ELS (right) measurements at half height of 5, 25 and 50 mgL^{-1} TiO_2 samples after 1, 4 and 24 h of incubation.

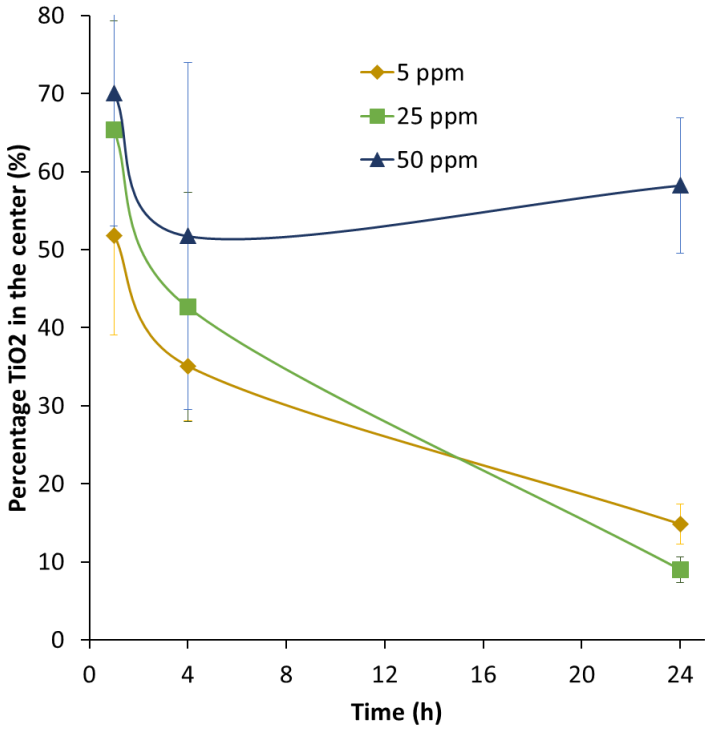

Figure 19: TiO_2 NPs concentration (%) at half height of water column for 5, 25 and 50 mg L^{-1} samples as a function of time (1, 4 and 24 h).

CONCLUSION

In this study we investigated the colloidal stability and sedimentation kinetic of $BaSO_4$,

CeO_2 and TiO_2 in 10% FBS biological media, mimicking the exposure conditions of in-vitro tests. The hydrodynamic diameter and Zeta Potential measured at half height of experimental set-up at different concentrations and time of exposure confirmed the high degree of agglomeration of NPs with different trend based on NPs nature. $BaSO_4$ NPs size values increase based on concentration, while ZP values were halved from 1h to 24h of exposure time. CeO_2 NPs size values present high polydispersity, increasing in time only for the higher concentration, and ZP values decrease as a function of exposure time, showing high agglomeration. TiO_2 NPs size distribution are not affected by time or concentration with high polydispersity, showing almost stable values (range 300 – 600 nm), while ZP values were reduced for all concentration after 24h of exposure. In front of the results achieved, the presence of FBS in medium should promote a stabilization of nano suspension for all kinds of NPs selected and, in some case, avoid the change in colloidal behaviour and in sedimentation as a function of concentration. However, the presence of the gelatine + GPTMS layer at the bottom of the experimental set-up, can influence the colloidal behaviour and sedimentation outcomes, absorbing NPs or partially dissolving in medium; thus, further evaluation is required to better understand the contribution of each parameter.

c. *Nano silver detection in tox media by SP-ICP-MS*

This study was focused on the evaluation of two different types of silver NPs (Ag NPs) behaviour in biological relevant media (DMEM and RPMI complete or not), by using single particle inductively coupled plasma mass spectrometry (SP-ICP-MS) technique to evaluate change in NPs size dimension and dissolution as a function of medium selected, concentration and exposure time. We selected Ag 300K NPs (Tier 1 PATROLS), Ø 15 nm and Ag NanoComposix, Ø 60 nm for the analysis.

SP-ICP-MS APPLIED TO AG 300K IN RPMI / RPMI + FBS (10%) / DMEM

Data were collected at the University of South Caroline (USC) facilities, where an ISTEC delegate spent 4 months for training and measurement generation. Data referring to Ag^+ ionic fraction and corresponding size diameter as calculated by SP-ICP-MS, after exposure of Ag 300K in RPMI / RPMI + FBS (10%) /DMEM, at 1h and 24h are reported in Table 11 and graphs of Figures 20–22.

Table 11: Data from SP-ICP-MS of Ag 300K incubated in different in vitro media at 24h

Concentration Ag 300K (ppb)	Media	Size (nm)	Dissolved Conc. Ag^+ (ppb)	Dissolution Ag^+/Ag tot %
50	RPMI	97 (±4)	12.82 (± 1.13)	25.6
	RPMI + FBS 10%	108 (±1)	16.38 (±0.91)	32.8
	DMEM complete	111 (±1)	16.10 (±0.36)	32.2
20	RPMI	77 (±2)	4.13 (± 0.52)	20.7
	RPMI + FBS 10%	95 (±2)	8.29 (±0.69)	41.5
	DMEM complete	92 (±1)	6.67 (±0.13)	33.4
10	RPMI	61 (±1)	1.77 (± 1.09)	17.7
	RPMI + FBS 10%	85 (±1)	5.48 (±0.20)	54.8
	DMEM complete	79 (±1)	3.69 (±0.05)	36.9
5	RPMI	53 (±1)	0.97 (± 0.11)	19.3
	RPMI + FBS 10%	82 (±2)	3.11 (±0.31)	62.2
	DMEM complete	67 (±2)	2.10 (±0.02)	42.0
1	RPMI	33 (±2)	0.11 (±0.01)	11.1
	RPMI + FBS 10%	47 (±1)	1.01 (±0.02)	100.0
	DMEM complete	46 (±4)	0.79 (±0.08)	79.0

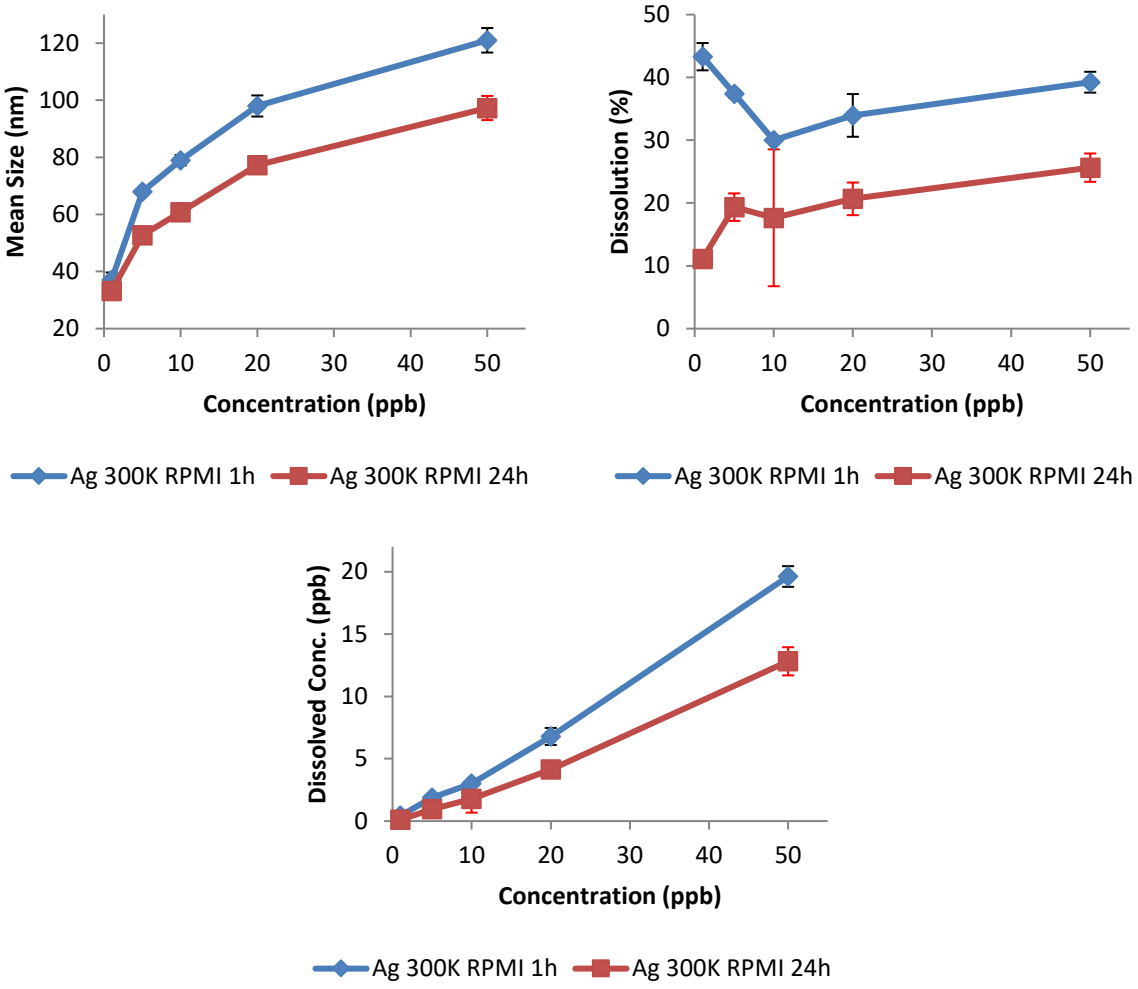

Figure 20. Size diameter and dissolved fraction of Ag 300K in RPMI media after 1h and 24h.

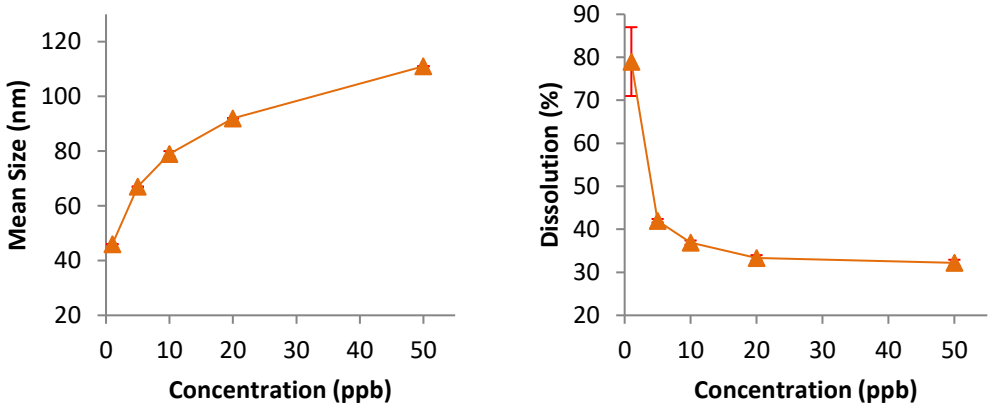

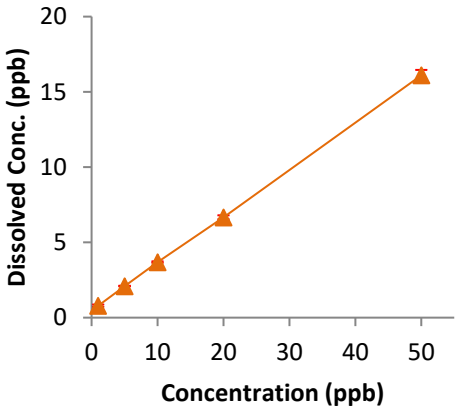

Figure 21: Size diameter and dissolution percentage of Ag 300K in DMEM + FBS (10%), after 24h.

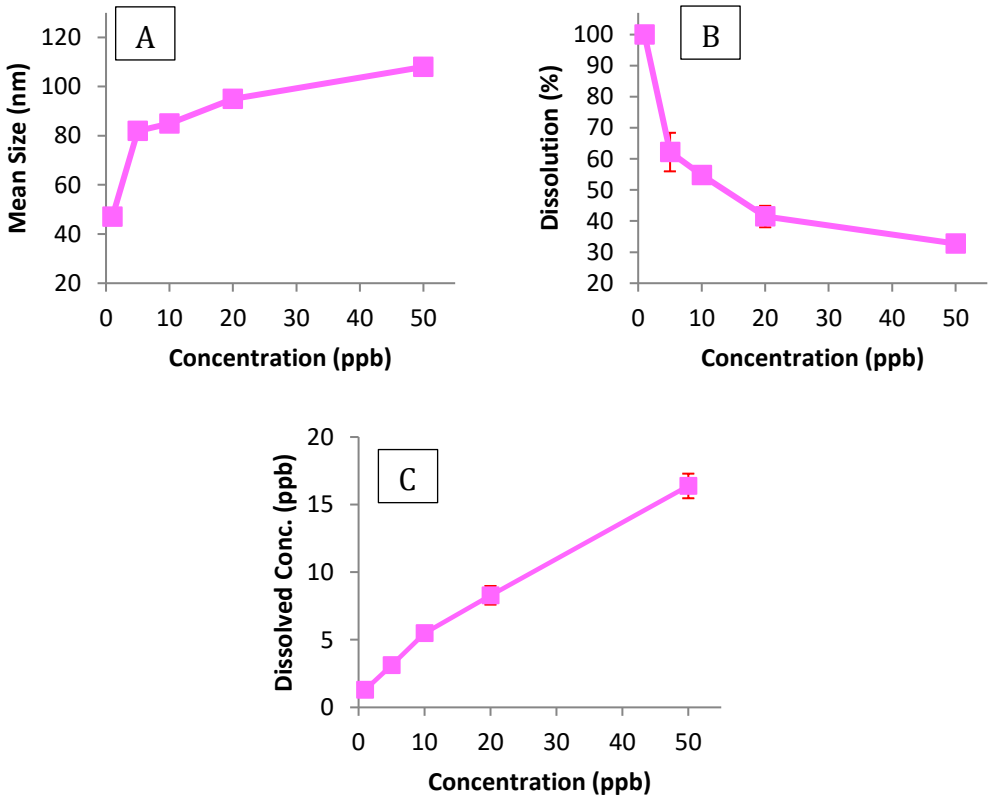

Figure 22: Size diameter (A), dissolution percentage (B) and dissolved fraction concetration (ppb) (C) of Ag 300K in RPMI + FBS (10%), after 24h.

When analyzing the data generated on the dissolution percentage and size of Ag 300 K, the main important result is that the estimated NPs size decreases, as expected, with decreasing concentration, approaching TEM size (< 20nm) at a very low concentration (below 5ppb). In RPMI, the dissolution expressed as Ag ppb detected is proportional to the sample starting concentration, indicating that samples under this very low concentration range did not reach the solubility limit.

The graphs referring to size and dissolution of Ag 300K after 24h of exposure, in *in vitro* complete media, DMEM and RPMI + FBS (10%), are similar. The dissolution, expressed as a percentage over the total, decreases from 80/100% to approximately 30%, whilst particle size increases passing from approximately 40/50 nm to 80/120 nm, when increasing the starting concentration, most likely due to the occurrence of aggregation phenomena. The differences found, if comparing RPMI with RPMI + FBS (10%), is something interesting that confirm how proteins (fetal bovine serum) are able to increase drastically the dissolved number of ions.

SP-ICP-MS APPLIED TO AG NANOCOMPOSIX IN RPMI / RPMI + FBS (10%) / DMEM

Ag NanoComposix was investigated as for the comparison with Ag 300K (PATROLS Tier 1 materials) because previous data had been collected by USC and were used for calibration purposes. Data referred to the Ag^+ ionic fraction and corresponding size diameter calculated by SP-ICP-MS, after exposure of Ag NanoComposix in RPMI, RPMI + FBS (10%) and DMEM, at 24h. The data is reported in Table 12 and Figure 23.

Table 12: Data from SP-ICP-MS of Ag NanoComposix incubated in different in vitro media at 24h.

Concentration Ag NanoComposix (ppb)	Media	Size (nm)	Dissolved Conc. Ag^+ (ppb)	Dissolution Ag^+/Ag tot %
50	RPMI	117 (±9)	39.84 (±4.64)	79.6
	RPMI + FBS 10%	104 (±1)	49.77 (±0.96)	99.5
	DMEM complete	104 (±1)	40.60 (±0.21)	77.3
20	RPMI	95 (±2)	16.68 (±1.98)	83.4
	RPMI + FBS 10%	89 (±1)	20.09 (±0.51)	100.0
	DMEM complete	89 (±1)	16.49 (±0.05)	82.4
10	RPMI	80 (±2)	6.93 (±1.09)	69.3
	RPMI + FBS 10%	79 (±1)	9.77 (±0.05)	97.7

	DMEM complete	78 (±1)	7.87 (±0.21)	78.7
5	RPMI	68 (±2)	2.99 (±0.71)	59.8
	RPMI + FBS 10%	68 (±1)	4.47 (±0.08)	89.4
	DMEM complete	68 (±1)	3.62 (±0.03)	72.4
1	RPMI	58 (±2)	0.20 (±0.06)	20.0
	RPMI + FBS 10%	56 (±1)	0.95 (±0.04)	95.0
	DMEM complete	55 (±1)	0.62 (±0.01)	62.0

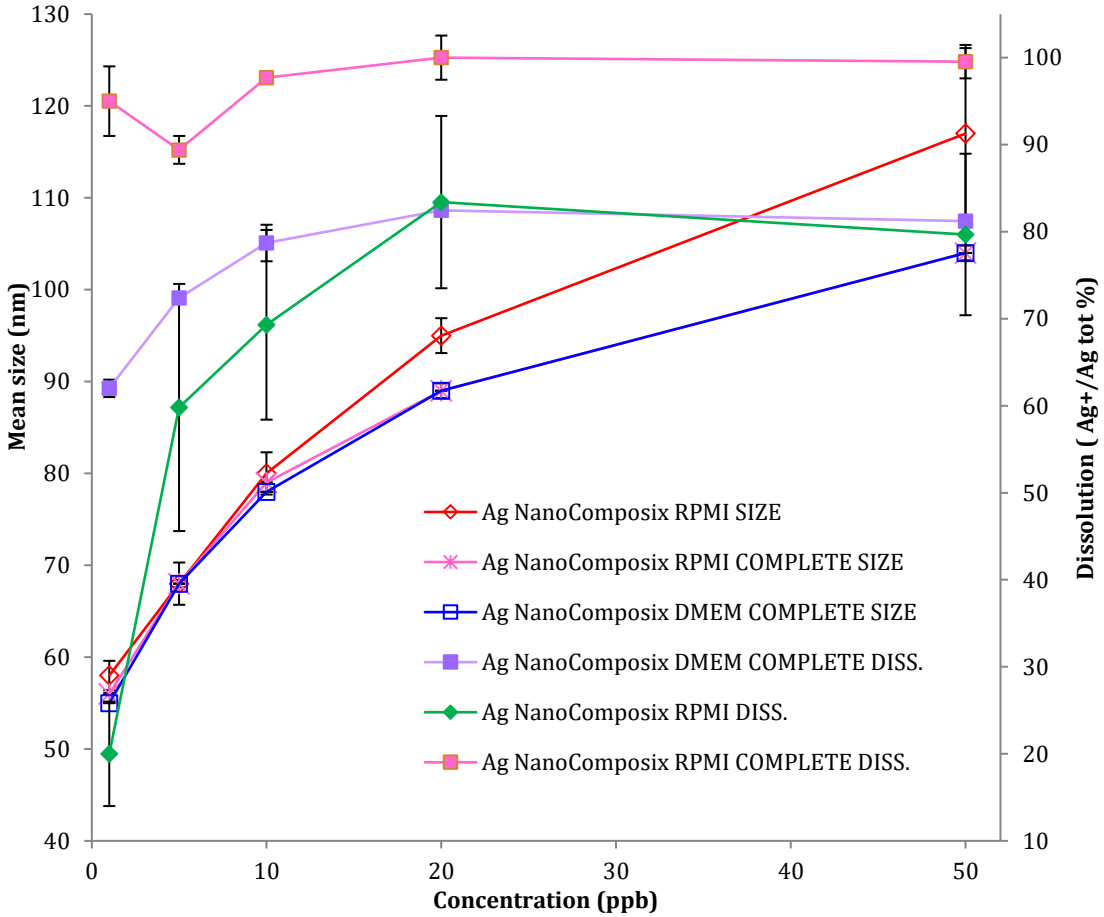

Figure 23: Mean size and dissolved fraction of Ag NanoComposix in different media

Comparing size and dissolution of another type of nanosilver (NanoComposix) in different media we noticed that size seems not to be affected by media, whilst the ions release is maximum in the presence of serum, reaching about 100% of dissolution in RPMI + FBS 10%. In RPMI medium without serum there is an abrupt decrease of dissolution below 10 ppb that passes from 80/90 % to 20% at 2 ppb.

CONCLUSION

This study allowed the direct measurement of particle size, particles and ions concentration at a low concentration range, corresponding to chronic long term exposure conditions. The main findings for Ag 300K were that the estimated NPs size decreases, by decreasing nominal concentration, approaching TEM size (< 20nnm) for very low concentration (below 5ppb); despite the results obtained by ICP-OES at higher concentration, that will be reported in Task 1.3, samples followed a dissolution of first order and did not reach the solubility limit.

2.2 Method documentation

a. *Materials and dispersion protocols*

The list of Tier 1 nanomaterials tested, with industrial providers and repositories where materials are stored, together with information available from providers or JRC reports, are reported in the Table below:

.

Tier 1	ENM & Supplier	Available form	Info available on Surface Properties / Morphology	Trade names, Company
1: Soluble (release possibly toxic ions)	ZnO (NM111; JRC) COATED	Powder	Capped (hydrophobic): (1%) Triethoxycaprylylsilane, XRD, 58-93 nm; SEM 140nm (OECD, 2015, 8); TEM: 101 ± 76 nm/170 ± 126; BET: 12.4 ± 0.6m2/g (Singh et al., 2011). **POSITIVE** (water, pH7)	Z-COTE® HP1, BASF, Germany
	ZnO (NM110; JRC) UNCOATED	Powder	Uncoated XRD, 71-100 nm; TEM: 106 ± 111 nm/178 ± 175 nm; BET: 15.1 ± 0.6m2/g (Singh et al., 2011). **POSITIVE** (water, pH7)	Z-COTE ®, BASF, Germany
	Ag (NM300K; Fraunhofer IME)	Suspension (10 wt.%)	Capped: Polyoxyethylene Glycerol Trioleate and Polyoxyethylene Sorbitan mono-Laurat , TEM < 20nm; DLS 50-170nm (JRC report 2011); **NEGATIVE** (pH7)	Ag Pure® W10, RAS AG, Germany.
2: Biopersistent HARN (fibre paradigm)	Mitsui-7 MWCNT (NRCWE-006)	Powder	Thick (70-170 nm) and long (1-19∝m), to be dispersed in BSA (OECD ENV/JM/MONO(2016)20) .	Mitsui & Co., Ltd., USA (catalyzed vapor deposition)
	MWCNT (NM402; JRC)	Powder	Thin (11 nm) and long (1372 nm), to be dispersed in BSA (JRC, Nanogenotrox report 2014) .	Arkema Graphistrength C100 (catalyzed vapor deposition)
3: Passive (negative, insoluble)	$BaSO_4$ (NM220; Fraunhofer IME)	Powder	Naked, 38 nm globular, strongly agglomerated (Nano Care project); **NEGATIVE** (pH7)	Solvay, Massa, Italy
4: Active (positive, insoluble; promote cellular effects and/or mobility in the organism)	CeO_2 (NM212; Fraunhofer IME)	Powder	Naked, XRD, 33nm; SEM 28nm (OECD, 2015, 8); **HIGHLY POSITIVE** (pH7)	Umicore (Hanau, Germany)
	SiO_2 crystalline quartz (DQ 12) SiO_2 amorphous (IUF)	Powder	Standard Dust in Silicosis (87% crystalline silica; *non-nanosized crystalline quartz DQ12, known to elicit pronounced effects in the lung upon inhalation exposure.* **HIGHLY POSITIVE** (pH7)	Crystalline silica (Robock, 1973) Amorphous silica from IUF is the Sigma, S5130 fumed silica
	TiO_2 (NM105; JRC)	Powder	Naked, formed by aggregates of several hundred nm in size and the primary particles have a mean diameter of approx. 21 nm (Evonik Data Sheet); **SLIGHTLY NEGATIVE** (pH7)	AEROXIDE® TiO2 P25

The following *in vitro* relevant media have been considered: Dulbecco Modified Eagle Medium (31053028, Gibco™, Thermo Fisher Scientific, Waltham, USA) + 10% Fetal Bovine Serum, (10500056, Gibco™ Thermo Fisher Scientific, Waltham, USA) + 1% Minimal Essential Medium (11140068, Gibco™, Thermo Fisher Scientific, Waltham, USA) + 1% Penicillin/Streptomycin 100x (15140122, Gibco™, Thermo Fisher Scientific, Waltham, USA) or RPMI (Rosewell Park Memorial Institute) (11835030, Gibco™, Thermo Fisher Scientific, Waltham, USA).

The dispersion approach taken in this set of experiments almost entirely relied on the Standard Operating Procedure (SOP) optimised by the NANoREG project, along with selected recommendations given by DeLoid et al. (DeLoid et al., 2017) for the preparation of stock suspensions, followed by flash freezing treatment in experiments discussed in Section 2.3. The goal was to use a workflow that was easy to replicate (see Figure S1), providing reproducible results. Any deviations from the SOP were

noted.

All available materials dictated by the PATROLS work plan were characterized, and each particle type was processed and characterized in independent triplicates. In summary, each particle type was weighed out according to the NANoREG SOP, to make a solution at a concentration of 2.56 mg/mL in 99.5 vol% sterile-filtered BSA-water (0.05% w/v), 0.5 vol% EtOH (96% pure). Each ENM was weighed out to be as close as possible to a total volume of 6 mL and placed in 30 mL Scint-Burk glass vials. The vials had the same diameter as the ones recommended by the NANoREG protocol and differ only in height, leading to an increased volume capacity. Subsequently, the material was prewetted by the appropriate EtOH volume, followed by the addition of the BSA solution, taking care to wash down the sides of the vial for material recovery. The BSA-water solution was prepared according to the NANoREG SOP.

NM-300K, NM-302 and Sigma Ag were all weighed out under argon atmosphere and stored under argon. NM-402 was weighed out using additional precautions: the weighing out was conducted in a hood specialized for Carbon NanoTube (CNT) use, using gloves and a 3M Aura Disposable Respirator (3M ID GT500073132, 3M Maplewood, USA). All other materials were weighed out using a separate calibrated scale. A Branson 550 probe sonicator equipped with a 3 mm tip was used for dispersion. The sonicator was calibrated following the protocol to deliver 7.35W, and all materials were sonicated for 16 minutes. The SOP was followed for calibration, with the only difference being that a volume of 200 mL of water was used. For the dispersions, care was taken to ensure that the tip of the sonicator was consistently submerged to a similar depth across samples, between the upper quarter and upper half of the volume. All solutions were submerged in an ice-water bath during sonication. Between samples, the tip of the sonicator was washed by sonication for 5 minutes in a 50:50 EtOH:DI H_2O solution, followed by rinsing by EtOH and air drying to prevent

cross-contamination.

Within 5 minutes following sonication, the dispersed particle solution was aliquoted into 1.5 mL microcentrifuge tubes (Eppendorf, 0030 120.191, Eppendorf AG, Hamburg, Germany) and flash-frozen in liquid nitrogen (LN_2). The tubes were pre-prepared by puncturing the cap with a small hole to prevent decompression at low temperatures. Cryo-protective gear, namely the use of gloves and long tweezers were used to protect the user, and all work was done in a chemical hood. The tubes were kept in LN_2 for at least 2 minutes, and then placed in long term storage at -80°C. The facilities at BASF do not have the standard -80°C freezers and thus we improvised by storing our samples in dry ice (-78.5°C).

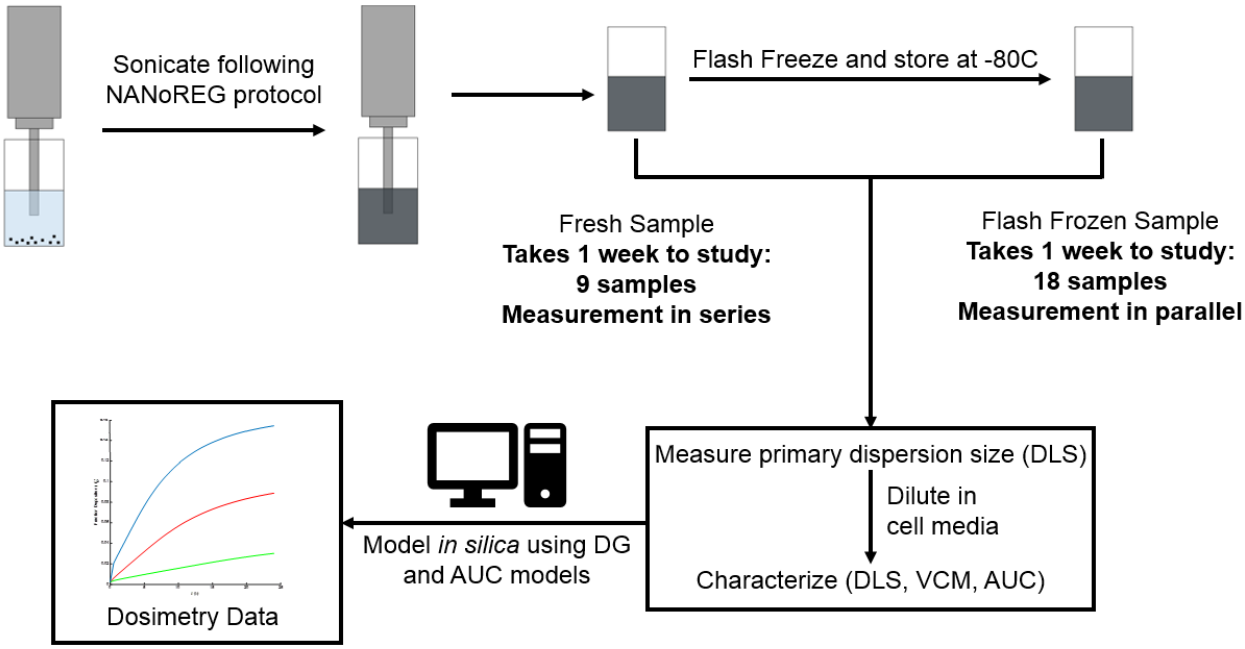

After flash freezing, each aliquot was thawed as needed. This was done by placing each aliquot in a hot (~65°C) bath sonicator for 1 minute, or until a small ice core was left in the tube. Immediately following thawing, the ENM suspensions were either measured or diluted 10x in MilliQ water (stock) and cell media, and incubated for 1 hour at 37°C. Sufficient sample was diluted for each intended application.

b. Dynamic Light Scattering (DLS)

After dispersion, the primary dispersions were diluted to a concentration of 0.256

mg/mL in relevant media and incubated at 37°C for 1 hour for subsequent physicochemical characterization. Flash-frozen samples were rapidly thawed in a 65°C bath sonicator until no ice crystals were left in the sample, and similarly diluted. Hydrodynamic size distributions of primary and cell media dispersions were measured using Dynamic Light Scattering (DLS) using a Malvern Zetasizer ZEN1600 (Malvern Panalytical Ltd. Malvern, United Kingdom). Instrument settings were set as dictated by the NANoREG SOP.

c. Analytical ultracentrifugation (AUC)

AUC implements an optical system that is synchronized with the centrifugal frequency to monitor the radial concentration profile during centrifugal separation. The samples were directly loaded in AUC cells without further preparation. All measurements were done on a Beckman Coulter XLI Proteome Lab (Beckman Coulter Inc., Brea, USA). The cells were all mounted on a 4-sample, or 8-sample, titanium rotor at 1000 rpm for 30 min, followed by 3000 rpm for 30 min and 12000 rpm for 2 h. The samples were measured using either interference or absorbance optics to detect sedimentation as described by the NanoDefine project.(Mehn, Rio-Echevarria et al. 2018) Both types of sedimentation data were evaluated with sedfit v15.0 software.

d. Testing of protein adsorption in batch dispersion and cDMEM mediums

The 16 nanomaterials selected for the PATROLS project, were all tested for adsorption of Lactate dehydrogenase (LDH), Interleukin-6 (IL-6) and Interleukin-8 (IL-8) in a mixture as follows.

Materials:

1. DMEM media (Gibco 41965-039)
2. Penicillin / streptomycin (Gibco 15140-122)
3. Foetal Bovine Serum (Brazil) (Gibco 10270-106)
4. Interleukin-6 standard 1µg (NIBCS code: 89/548)

5. Interleukin-8 standard 1µg (NIBCS code: 89/520)
6. L-LDH from rabbit mucle (5 mg/mL) (Sigma-Aldrich: 10127230001)
7. 0,05 % BSA (as described above)
8. 24-well plates (Greiner)

Nanomaterials, 0,05% BSA and DMEM working solution is added to a 24-well plate (one material per plate) in duplicates as described below (Protein concentration per well: IL-6 375 pg, IL-8 3000 pg, LDH 75 ng)

Particle concentration µg/mL	NM 2,56 mg/mL µL/well	0,05% BSA µL/well	DMEM working solution µL/well
0	0,0	250,0	750
10	3,9	246,1	750
20	7,8	242,1	750
40	15,6	234,4	750
80	31,3	218,8	750
160	62,5	187,5	750
320	125,0	125,0	750
640	250,0	0,0	750

The plate was incubated in a CO_2-incubator for 24 hours. After incubation, the replicates were harvested and transferred to Eppendorf vials and centrifuged at 20000 rpm for 30 minutes. After centrifugation, the supernatants were transferred to new Eppendorf vials and kept in the refrigerator until the following day.

LDH measurement:

LDH should be measured the same day as harvesting or at the latest the day after. In this case, all LDH measurements were performed the day after harvesting. After LDH measurement, the samples were kept at minus 20 °C until interleukin measurement.

Kit test: LDH Cytotoxicity Detection Kit fra Roche (Catalog no. Sigma 11644793001)

Protein measurement:

The total concentration of protein were measured in the material dispersions (after

sonication), the 0,05% BSA water, the pure DMEM media (without pen/strep and FBS) and in the DMEM working solution.

Kit test: Pierce BCA Protein Assay Kit (Thermo Scientific catalog no. 23227)

IL-6 and IL-8 measurement:

The frozen supernatants were thawed, and interleukin 6 and 8 were measured. The two assays are very similar, so both interleukins were analysed simultaneously.

Kit test: Human IL-6 ELISA Set (BD Bioscience catalog no. 555220)

Human IL-8 ELISA Set (BD Bioscience catalog no. 555244).

e. Sequential incubation studies

Media:

The composition of IUF_S, IUF_I, LSF and PSF simulant fluids is given in the appendix (*Table S1*). Note that the two steps of the IUF protocol, IUF_S and IUF_I are inseparable, and in the following tables this treatment is listed simply as “IUF”, which always represents both steps. The IUF pre-treatment protocol explicitly states that no sonication should be used in the sample preparation process. Due to the low shear, the focus of the analysis can then be aimed towards the influence of the different media but not the comparison of different *in vivo* scenarios.

Incubation protocol:

The ENM is added to the first medium to obtain a concentration of 4 mg/mL. The dispersion is then stirred two times for one hour at 350 rpm and a temperature of 37 °C. This seemingly odd procedure ensures analogous conditions as in the IUF pre-treatment (which is a two-step process) for all other media. The size distribution of an aliquot of the sample is then measured by AUC following the NanoDefine protocol.(Mehn, Rio-Echevarria et al. 2018) Another aliquot is filtered through a 5 kDa filter and the dissolved ions are measured with ICP-MS.

In the next step, the second medium is added at a ratio of 10:1. The excess is important

to minimize influences of the previous medium, concerning pH and all other parameters. Similar ratios are used by sequential testing of GIT dissolution.(Bove, Malvindi et al. 2017) The sample is then dispersed through ultrasonic power at an amplitude of 25% and a sonication duration of one minute. A Branson 550 tip sonicator was used for the sonication (Branson 550 (550W), Branson Ultrasonics Corp., Danbury, CT, USA). As an alternative process, the mixing of the sample could be done by stirring only. However, then agglomerates would not be given the chance to restructure by the interactions with their newly formed adsorbates, after being broken up by sonication. Hence for this approach high shear is used. After sonication the sample is stirred and measured as above by each one aliquot for AUC and ICPMS. The aim is to identify the effects of a hard corona which controls the uptake of particles in sequential compartments.

f. Dosimetry by sedimentation transport

The raw sedimentation coefficients measured by the AUC, as fitted by sedfit software, does not require any assumptions about particle size, density or composition. Instead, the measured distribution of sedimentation coefficients can be directly used to calculate the deposited dose. Dosimetry for all measured materials was calculated using either AUC calculated sedimentation driven transport or the DG model. The AUC coefficient was converted through integration to sedimentation driven transport and delivered dose using methods described in (Sauer, Aumann et al. 2015, Wohlleben, Coleman et al. 2019).

g. Dosimetry by DG Model calculation (input parameters)

The principle of DG modelling relies on a successive modelling of diffusion and sedimentation based on the media height, with variable heights of the sub-compartment from run to run, and the particle size distribution. The iterative modelling also accounts for the stickiness of the bottom of the wells, which can be tuned

accordingly. The adjustable input parameters used for testing the DG model are listed in the table below:

Adjustable parameters used in the DG model simulations.

Parameter	Value used	
Solvent dynamic viscosity	0.00081 Pa·s	
Media density	0.9995 g/cm3	
Temperature	37°C	
Effective density	Measured, values used described in each experiment (units: g/cm3)	
Size distribution	Measured, values used described in each experiment. All experiments used 1-hour media incubation measurement (units: nm)	
*Media height	4 mm (media height above the top cell layer in a 12 well Transwell insert.)	
*Initial material concentration	0.256 mg/cm3 (unless otherwise noted. This value is the highest concentration dictated by the NANoREG SOP.)	
*Simulation time	24 hours	
Gravity	1 g	
Height of simulation sub-compartment	0.005 mm	
Simulation time interval	0.5 s	
Output Parameters		
Output data time intervals	30 min	
Output compartment height	0.0005 mm	
Adsorption dissociation constant (Kd)	Boundary Condition	Value (M)
	Adhesive	1x10-9
	Non-Adhesive	1x10-8
	Reflective	None, function turned off

h. DG model experimental validation (concentration at half column height)

Stocks, for $BaSO_4$ (NM-220), CeO_2 (NM-212) and TiO_2 (NM-105), were prepared following the NANOREG protocol in BSA medium. Then the stocks were diluted in MilliQ + 10% FBS medium reaching the concentration of 5, 25 and 50 mg L-1. To mimic the well plate conditions of in-vitro tests at a bigger scale, we designed and developed the experimental set-up of 8 mL reported in Figure S1.

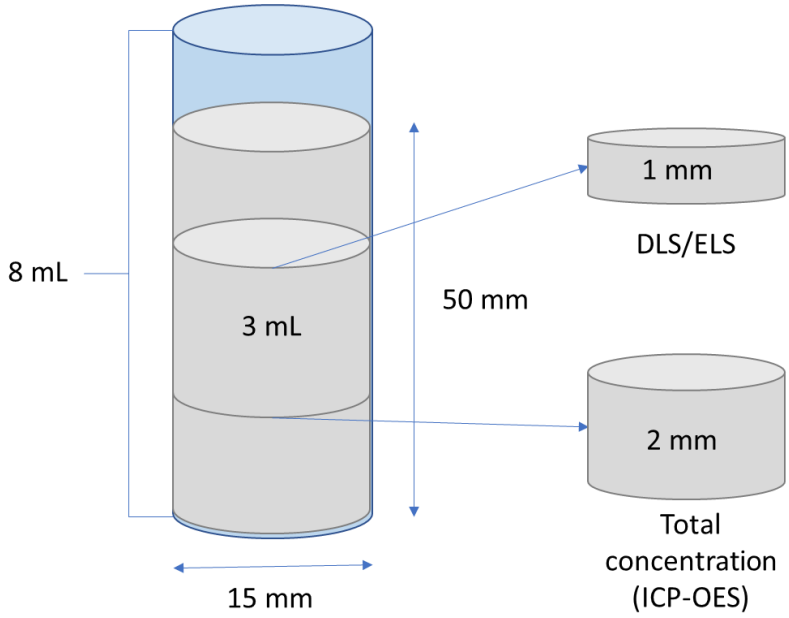

Figure S1: experimental set-up for the measurement of the colloidal behaviour (DLS/ELS) and concentration of NPs at half height of water column.

The layer of gelatine + GPTMS on the bottom of the experimental set-up was prepared starting, from a solution of gelatine type A 1% w/v in deionized water. The solution was stirred for about 30 minutes on the at 70 °C, then add GPTMS in ratio 100 µL per gram of gelatine dissolved in the solution. Stir the solution at 70 °C for other 30 minutes. To obtain the thickness similar to a layer of cells, we poured 626 µL of the solution (gelatine + GPTMS) into the experimental cylindric set-up and allowed to evaporate at 37 °C for 36 h. Before starting the experiment, we hydrated the film obtained after evaporation with 500 µL MilliQ water for 10 minutes and then removed it. DLS/ELS and ICP-OES measurements were performed on the 3 mL collected at half height of the water column, obtaining size distribution, zeta potential and concentration of NPs information. To study the sedimentation, the NPs concentration at half height were expressed as percentage of NPs / NPs dispersed in the column at time 0 hour.

Samples were incubated in static conditions at 38°C and collected after 0, 1, 4 and 24 hours. Each sample was used once and done in triplicate.

i. SP-ICP-MS instrumentation and working conditions

The SP-ICP-MS analysis were run using the Nano Application Module in Syngisitx™ software (version 2.1). A pump speed 20 rpm for flush, wash and delay, and nebulizer gas flow of 1.12 mL min−1 were used for measurements. The sample uptake was 0.34 mL min−1 and a dwell time of 50 µs was used with 60 s sampling times. To calculate the transport efficiency (1, 5 and 10 µg L-1) an ionic Au standard was used for SP-ICP-MS ionic calibration (ion mass 197 a.m.u.). While Au 60 nm NPs citrate coated suspension were used as standard for NPs size dimension in single-particle software calibration material. The 60 nm Au particles were diluted in MilliQ water to approximately 50,000 particles number mL−1 for SP-ICP-MS size calibration. We calculated a transport efficiency of 9.3 ± 2.5%. NPs dimensions detectable by SP-ICP-MS is a NPs dimension > 15 nm. Data analysis was performed with Excel for Windows, release 2007. All standards used were purchased from Sigma Aldrich (Milan, Italy).

3. Deviations from the Workplan

No significant deviation from the workplan occurred. The results of the evolution of the surface and bulk composition in (eco) tox relevant media by XPS and PIXE techniques (UNamur) will be delivered in D1.5 because it is an important element required to complete the study of dosimetry and fate in ecotoxicity testing environments. Foreseen tests on powder samples: dustiness tests and hydrophobicity/hydrophilicity tests with sessile water drop contact angle were not done because it was considered less relevant for the 3D models developed by PATROLS. Instead, much greater focus was given to the parametrisation and experimental validation of sedimentation/diffusion dosimetry models, in collaboration with WP6.

4. Performance of the partners

BASF and ISTEC investigated the agglomeration state through DLS measurements in water and different cell culture media containing serum to evaluate their stability and the impact of different storing conditions upon this stability. In particular, BASF and ISTEC tested the suitability of the flash freezing procedure, suggested by BASF, to prepare stock suspensions that can be stored and used for multiple measurements, over time. ISTEC completed the colloidal characterization (DLS mean diameter and ELS Zeta potential) of fresh (FR), freeze-thawed (FT) and aged (A) suspensions, whilst BASF used these as input data for the DG dosimetry model in order to consider how potential changes in particle size distribution could affect the fraction of deposited dose vs time. NRCWE investigated the interaction between test materials and the cytokines and LDH secreted from cells during inflammation and cell membrane leakage. Depletion analysis tests were performed to establish the amount of LDH adsorbed onto NPs. ISTEC performed intensive DLS/ Zeta potential campaigns (Tier 1 materials, different concentrations and times of exposure) in eco-tox media, whilst UNamur

investigated their stability through the centrifugal liquid sedimentation (CLS) technique; however, we have decided to merge all these results in D1.5. BASF designed a pre-treatments and sequential incubation study to track the exposure identity of NPs when they translocate through several physiological compartments, after inhalation and oral exposure. The surface chemistry transformation was evaluated by EDX and XPS, ions dissolution was measured after ultrafiltration by ICP-MS, whilst particle size distribution was characterised using AUC.

BASF tested the *in silico* dosimetry model Distorted Grid (DG), comparing sedimentation rate calculated by the model with that empirically detected by the analytical ultracentrifugation (AUC) technique. In particular, they tested the effects of freeze-thawing treatment, variability between triplicates, different thermodynamic boundary conditions (stickiness), different methods used to provide size distribution and the overall modelling consistency. They identified the most sensitive parameters affecting results and provided very useful information to understand the limitations of the currently widely used dosimetry prediction models, indicating solutions for significantly enhanced accuracy. ISTEC extended measurements to further cell culture media and *in vitro* testing conditions, and provided experimental validation of the dosimetry model by measuring the concentration of ENM at half column height of the *in vitro* testing systems. Finally, ISTEC in collaboration with USC measured the total concentration, the ionic fraction and particle size distribution of Ag NPs, dispersed in different "*in vitro*" media, at different concentrations, representative of long-term exposure studies (ppb).

5. Conclusions

The work done in this task assessed two main aspects in the evaluation of nanoparticles' transformation and behaviour in toxicologically relevant media: how the sample dispersion governs the exposure identity and how the dose is effectively delivered to the final biological target. These two aspects are essential to monitor and understand phenomena, that occur at the nano-liquid interface, and establish a dose-response output.

The evaluation of exposure identity was investigated through different approaches. Firstly, for the study of differences in dispersion protocols, Fresh / Freeze-thawed / Aged suspensions were compared. DLS size and ELS Zeta potential were compared, and the suitability of freeze-thawing treatment was also tested, by deriving the fraction of sedimented dose vs time through the Distorted Grid (DG) dosimetry model. Some samples like Ag NM300K, Ag Sigma, $BaSO_4$, SiO_2 NM200 seem to be only slightly affected by freezing (-80°C) or ageing at storing condition (4°C); otherwise, samples such as MWCNTs NM402 and Mitsui are dramatically destabilized; while samples like TiO_2 and ZnO are only partially modified and in general result in more aggregation after freeze-thawing treatment. Overall, considering the advantages that freeze-thawing treatment can provide for speeding the characterizations process, we can conclude that this can be considered a good option to save time and allow a better comparison between samples prepared at different times. Depletion analysis allowed the establishment of the amount of LDH adsorbed onto NPs surface, highlighting different behaviours between particle composition. The LDH adsorption is highly similar between the three ZnO materials evaluated, ending at around 60% loss of all LDH available in the medium. The silver materials displayed two different adsorption

phenomena. A very high loss was observed at low particle doses of Ag-Sigma while a slower adsorption rate was observed for Ag-JRC (NM-302). Carbon nanotubes only showed limited adsorption of LDH. Pre-treatments and sequential incubation studies were used to investigate the NPs transformation and transport related processes, that occur when they pass through different biological compartments, as happens when they are circulated in the human body. The results showed that for a metal oxide, with limited options of chemical transformation, the sequential incubation is an unnecessary complication of the sample preparation, because it leaves little traces on the material. The same result would be obtained by directly dispersing the material into the medium that is relevant to the cells. In contrast, a reactive material such as Ag Sigma showed large differences by sequential incubation as compared to single media. The sample remained almost frozen in the state of agglomeration induced by the first medium. This means that for a reactive material, the exposure identity is formed by the pre-treatments, which are a means to design “what” is exposed onto the cells. Regarding dosimetry, the fundamental notion that the deposited dose is lower than the total administered dose was easily supported by simple measurements (DLS, VCM) and DG modelling. What we found is that the prediction of deposited dose varies significantly, with a deposited dose ranging between 9-73% for the different ENMs, adopting reflective boundary conditions in the DG model. Especially for well dispersed ENMs, uncertainty is introduced by selecting an arbitrary choice of affinity of particles to cells (“reflective” vs. “adhesive” bottom). Additionally, for polydisperse ENMs, minor details of the particle size distribution strongly influence the modelled dosimetry, such that the choice of the measurement technique (e.g. DLS or AUC) introduces further uncertainties to the dosimetry modelling. For any polydispersed ENM, we found it necessary to increase the DG model computing resources by reducing the output compartment height to 0.0005 mm; otherwise, dips in the particle settling traces lead

to erroneous predictions. The further development and experimental validation of DG model, performed in collaboration with WP6, by comparing the calculated and measured concentration at half column height, showed a good encouraging correlation between calculated and measured data. Finally, in addition, the use of the latest analytical technique, SP-ICP-MS, promotes the detection of NPs in toxicological media. The characterisation of AgNPs in *in vitro* testing media allowed the direct measurement of particle size, particles and ions concentration, at a low concentration range, corresponding to chronic long term exposure conditions. The main findings for Ag 300K were that the estimated NPs size decreases, by decreasing nominal concentration, approaching TEM size (< 20nnm) for very low concentration (below 5ppb); samples followed a dissolution of first order and did not reach the solubility limit. All these results comprise a comprehensive investigation of the NPs real dose and form, which comes into contact with the biological targets, providing a robust and more realistic approach for exposed dose prediction.

The Steering Board deems this deliverable to be complete and acceptable for submission.

6. Annex

Table S1: Media Composition of physiological relevant fluids, IUF_S, IUF_I, LSF, PSF.

IUF_S (Gastric Solution) pH 2.7		[mg/L]
Sodium chloride	NaCl	1980
Hydrochloric acid	HCl	to pH 2.7

IUF_I (Intestinal Solution) pH 9.5		[mg/L]
Sodium chloride	NaCl	2000
Sodium hydrogen carbonate	$NaHCO_3$	3580
Disodium carbonate	Na_2CO3	840

PSF (Stefaniak et al.) pH 4.5		[mg/L]
Sodium phosphate dibasic anhydrous	Na_2HPO_4	171
Sodium chloride	NaCl	6650
Sodium sulfate anhydrous	Na_2SO_4	71
Calcium chloride dehydrate	$CaCl_2x2H_2O$	29
Glycine	$C_2H_5NO_2$	450
Potassium hydrogen phthalate	$(1\text{-}(HO_2C)\text{-}2\text{-}CO_2K)\text{-}C_6H_4)$	4084.6
Alkylbenzyldimethylammonium chloride	(ABDC)	50

LSF (Modified Gamble (citrate)) pH7.4		[mg/L]
Sodium Chloride	NaCl	3208
Sodium Hydroxide	NaOH	1888
Citric Acid xH2O	Citric Acid xH2O	5424
Calcium chloride dehydrate	$CaCl_2x2H_2O$	29
Sodium phosphate dibasic anhydrous	Na_2HPO_4	171
Sodium sulfate anhydrous	Na_2SO_4	40
Magnesium Chloride	MgCl2x6H2O	106
Glycine	$C_2H_5NO_2$	59
Trisodium citrate	Na3citrate x2H2O	76
Sodium tartrate	Na2tartrate x2H2O	90
Sodium pyruvate	Na-pyruvate	86
90% lactic acid	$C_3H_6O_3$	79

6. References

Arts, J.H.E., Irfan, M.-A., Keene, A.M., Kreiling, R., Lyon, D., Maier, M., Michel, K., Neubauer, N., Petry, T., Sauer, U.G., Warheit, D., Wiench, K., Wohlleben, W., Landsiedel, R., 2016. Case studies putting the decision-making framework for the grouping and testing of nanomaterials (DF4nanoGrouping) into practice. Regulatory Toxicology and Pharmacology 76, 234–261. https://doi.org/10.1016/j.yrtph.2015.11.020

Bihari, P., Vippola, M., Schultes, S., Praetner, M., Khandoga, A.G., Reichel, C.A., Coester, C., Tuomi, T., Rehberg, M., Krombach, F., 2008. Optimized dispersion of nanoparticles for biological in vitro and in vivo studies. Part Fibre Toxicol 5, 14.

https://doi.org/10.1186/1743-8977-5-14

Bove, P., Malvindi, M.A., Kote, S.S., Bertorelli, R., Summa, M., Sabella, S., 2017. Dissolution test for risk assessment of nanoparticles: a pilot study. Nanoscale 9, 6315–6326. https://doi.org/10.1039/c6nr08131b

Cohen, J.M., Teeguarden, J.G., Demokritou, P., 2014. An integrated approach for the in vitro dosimetry of engineered nanomaterials. Part Fibre Toxicol 11, 20. https://doi.org/10.1186/1743-8977-11-20

Da Silva, E., Kembouche, Y., Tegner, U., Baun, A., Jensen, K.A., 2019. Interaction of biologically relevant proteins with ZnO nanomaterials: A confounding factor for in vitro toxicity endpoints. Toxicology in Vitro 56, 41–51. https://doi.org/10.1016/j.tiv.2018.12.016

Danielsen, P.H., Møller, P., Jensen, K.A., Sharma, A.K., Wallin, H., Bossi, R., Autrup, H., Mølhave, L., Ravanat, J.-L., Briedé, J.J., de Kok, T.M., Loft, S., 2011. Oxidative Stress, DNA Damage, and Inflammation Induced by Ambient Air and Wood Smoke Particulate Matter in Human A549 and THP-1 Cell Lines. Chem. Res. Toxicol. 24, 168–184. https://doi.org/10.1021/tx100407m

DeLoid, G.M., Cohen, J.M., Pyrgiotakis, G., Demokritou, P., 2017. Preparation, characterization, and in vitro dosimetry of dispersed, engineered nanomaterials. Nat Protoc 12, 355–371. https://doi.org/10.1038/nprot.2016.172

DeLoid, G.M., Cohen, J.M., Pyrgiotakis, G., Pirela, S.V., Pal, A., Liu, J., Srebric, J., Demokritou, P., 2015. Advanced computational modeling for in vitro nanomaterial dosimetry. Part Fibre Toxicol 12, 32. https://doi.org/10.1186/s12989-015-0109-1

Gray, E.P., Browning, C.L., Wang, M., Gion, K.D., Chao, E.Y., Koski, K.J., Kane, A.B., Hurt, R.H., 2018. Biodissolution and cellular response to MoO3 nanoribbons and a new framework for early hazard screening for 2D materials. Environ. Sci.: Nano 5, 2545–2559. https://doi.org/10.1039/C8EN00362A

Gubala, V., Johnston, L.J., Krug, H.F., Moore, C.J., Ober, C.K., Schwenk, M., Vert, M., 2018. Engineered nanomaterials and human health: Part 2. Applications and nanotoxicology (IUPAC Technical Report). Pure and Applied Chemistry 90, 1325–1356. https://doi.org/10.1515/pac-2017-0102

Hadrup, N., Bengtson, S., Jacobsen, N.R., Jackson, P., Nocun, M., Saber, A.T., Jensen, K.A., Wallin, H., Vogel, U., 2017. Influence of dispersion medium on nanomaterial-induced pulmonary inflammation and DNA strand breaks: investigation of carbon black, carbon nanotubes and three titanium dioxide nanoparticles. Mutagenesis 32, 581–597. https://doi.org/10.1093/mutage/gex042

Hartmann, N.B., Jensen, K.A., Baun, A., Rasmussen, K., Rauscher, H., Tantra, R., Cupi, D., Gilliland, D., Pianella, F., Sintes, J.M.R., 2015. Techniques and Protocols for Dispersing Nanoparticle Powders in Aqueous Media—Is there a Rationale for Harmonization? Journal of Toxicology and Environmental Health, Part B 18, 299–326. https://doi.org/10.1080/10937404.2015.1074969

Jacobsen, N.R., Møller, P., Jensen, K.A., Vogel, U., Ladefoged, O., Loft, S., Wallin, H., 2009. Lung inflammation and genotoxicity following pulmonary exposure to nanoparticles in ApoE-/- mice. Particle and Fibre Toxicology 6, 2. https://doi.org/10.1186/1743-8977-6-2

Krug, H.F., 2014. Nanosafety Research—Are We on the Right Track? Angewandte Chemie International Edition 53, 12304–12319. https://doi.org/10.1002/anie.201403367

Lin, M.Y., Lindsay, H.M., Weitz, D.A., Ball, R.C., Klein, R., Meakin, P., 1990. Universal reaction-limited colloid aggregation. Phys. Rev. A 41, 2005–2020. https://doi.org/10.1103/PhysRevA.41.2005

Lison, D., Thomassen, L.C.J., Rabolli, V., Gonzalez, L., Napierska, D., Seo, J.W., Kirsch-Volders, M., Hoet, P., Kirschhock, C.E.A., Martens, J.A., 2008. Nominal and

effective dosimetry of silica nanoparticles in cytotoxicity assays. Toxicol. Sci. 104, 155–162. https://doi.org/10.1093/toxsci/kfn072

Marucco, A., Aldieri, E., Leinardi, R., Bergamaschi, E., Riganti, C., Fenoglio, I., 2019. Applicability and Limitations in the Characterization of Poly-Dispersed Engineered Nanomaterials in Cell Media by Dynamic Light Scattering (DLS). Materials 12, 3833. https://doi.org/10.3390/ma12233833

Milani, S., Baldelli Bombelli, F., Pitek, A.S., Dawson, K.A., Rädler, J., 2012. Reversible versus Irreversible Binding of Transferrin to Polystyrene Nanoparticles: Soft and Hard Corona. ACS Nano 6, 2532–2541. https://doi.org/10.1021/nn204951s

Monopoli, M.P., Aberg, C., Salvati, A., Dawson, K.A., 2012. Biomolecular coronas provide the biological identity of nanosized materials. Nat Nanotechnol 7, 779–786. https://doi.org/10.1038/nnano.2012.207

Monteiro-Riviere, N.A., Tran, C.L., 2014. Nanotoxicology: Progress toward Nanomedicine, Second Edition, 2 edizione. ed. CRC Press.

NANoREG D2 06 DR Validated protocols for test item preparation for key in vitro and ecotoxicity studies | RIVM [WWW Document], n.d. URL https://www.rivm.nl/en/documenten/nanoreg-d2-06-dr-validated-protocols-for-test-item-preparation-for-key-in-vitro-and (accessed 4.7.20).

Petersen, E.J., Bustos, A.R.M., Toman, B., Johnson, M.E., Ellefson, M., Caceres, G.C., Neuer, A.L., Chan, Q., Kemling, J.W., Mader, B., Murphy, K., Roesslein, M., 2019. Determining what really counts: modeling and measuring nanoparticle number concentrations. Environ. Sci.: Nano 6, 2876–2896. https://doi.org/10.1039/C9EN00462A

Schulze, C., Schulze, C., Kroll, A., Schulze, C., Kroll, A., Lehr, C.-M., Schäfer, U.F., Becker, K., Schnekenburger, J., Isfort, C.S., Landsiedel, R., Wohlleben, W., 2008. Not ready to use – overcoming pitfalls when dispersing nanoparticles in physiological

media. Nanotoxicology 2, 51–61. https://doi.org/10.1080/17435390802018378

Teeguarden, J.G., Hinderliter, P.M., Orr, G., Thrall, B.D., Pounds, J.G., 2007. Particokinetics in vitro: dosimetry considerations for in vitro nanoparticle toxicity assessments. Toxicological sciences : an official journal of the Society of Toxicology. https://doi.org/10.1093/toxsci/kfl165

Vila, L., Rubio, L., Annangi, B., García-Rodríguez, A., Marcos, R., Hernández, A., 2017. Frozen dispersions of nanomaterials are a useful operational procedure in nanotoxicology. Nanotoxicology 11, 31–40. https://doi.org/10.1080/17435390.2016.1262918

Vranic, S., Gosens, I., Jacobsen, N.R., Jensen, K.A., Bokkers, B., Kermanizadeh, A., Stone, V., Baeza-Squiban, A., Cassee, F.R., Tran, L., Boland, S., 2017. Impact of serum as a dispersion agent for in vitro and in vivo toxicological assessments of TiO2 nanoparticles. Arch. Toxicol. 91, 353–363. https://doi.org/10.1007/s00204-016-1673-3

Walczyk, D., Bombelli, F.B., Monopoli, M.P., Lynch, I., Dawson, K.A., 2010. What the Cell “Sees” in Bionanoscience. J. Am. Chem. Soc. 132, 5761–5768. https://doi.org/10.1021/ja910675v

Wohlleben, W., 2012. Validity range of centrifuges for the regulation of nanomaterials: from classification to as-tested coronas. J Nanopart Res 14, 1300. https://doi.org/10.1007/s11051-012-1300-z